PRIFYSGOL
BANGOR
UNIVERSITY

Residual flow, bedforms and sediment transport in a tidal channel modelled with variable bed roughness

Davies, Alan; Robins, Peter

Geomorphology

Peer reviewed version

Cyswllt i'r cyhoeddiad / Link to publication

09. Oct. 2020

Accepted Manuscript

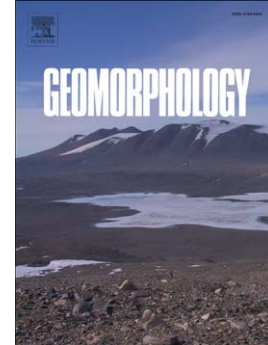Residual flow, bedforms and sediment transport in a tidal channel modelled with variable bed roughness

A.G. Davies, P.E. Robins

Residual flow, bedforms and sediment transport in a tidal channel

modelled with variable bed roughness

A.G. Davies[*] and P.E. Robins

Centre for Applied Marine Sciences, School of Ocean Sciences, Bangor University, Menai Bridge, Anglesey LL59 5AB U.K.

[*] Corresponding author: Email: a.g.davies@bangor.ac.uk; Tel +44 (0)1248 383933

Abstract

The frictional influence of the seabed on the tidal flow in shelf seas and estuaries is usually modelled via a prescribed, spatially/temporally invariant drag coefficient. In practice, the seabed exhibits considerable variability, particularly spatially, that should in principle be included in simulations. Local variations in the seabed roughness (k_s) alter the flow strength and, hence, local sediment transport rates. The effect of using a spatially/temporally varying k_s is assessed here with reference to a tidal channel (Menai Strait, N. Wales) in which the variability of the bedforms has been monitored using multi-beam surveying. The channel not only exhibits strong tidal flow, but also a residual induced flow that is used here as diagnostic to assess various bed roughness formulations tested in a Telemac model. Tidal simulations have been carried out with both constant and temporally/spatially variable k_s, and the predicted residual flow is shown to be sensitive to these representations. For a mean spring-neap (SN) cycle with variable k_s, the average residual flow is calculated to be 525 $m^3\,s^{-1}$, consistent with observations. This residual flow can be recovered using imposed, constant values of k_s in the range 0.15 m to 0.3 m. The results suggest that the overall, effective roughness of the seabed is less than half of the maximum local roughness due to the dunes in mid-channel, but more than the spatially-averaged k_s value in the channel as a whole by about 50%. Simulations carried out with an M_2-alone tide using variable k_s produce a somewhat smaller (by 7%) residual flow of 491 $m^3\,s^{-1}$. The use of an 'equivalent

1

M_2' tide of amplitude enhanced by 7.3% reconciles these estimates. The main contribution to k_s is made by dunes which are modelled using Van Rijn's (2007) formulation subject to an additional 'history effect'. The modelled k_s is found to equal approximately the observed height of the dunes along mid-channel transects rather than half the height as expected. This is attributed to the non-equilibrium nature of the bedforms in the reversing tidal flow, which exhibited shorter wavelength and more symmetrical profiles than dunes in steady flow.

Keywords: Variable seabed roughness; Sand dune roughness; Tidal friction; Induced tidal residual; Net sediment transport rate; Menai Strait, N. Wales.

2

1. Introduction

The presence of dunes on a mobile channel bed influences the hydraulic roughness, water levels and flow rates. Most studies of these effects have involved rivers where the slowly varying roughness k_s of the main channel is sometimes used as a calibration parameter to match observed water levels. In contrast, in tidal environments temporal variations in the flow typically occur more rapidly than the associated roughness of the bedforms, requiring 'history' or 'relaxation' methods to define k_s. The sophistication with which the seabed can now be mapped on fine spatial scales challenges modellers to improve the representation of bed features in estuarine and coastal area models. The seabed roughness k_s influences the flow strength, turbulent mixing, bed shear stress, sediment flux and, hence, the morphodynamic development of the bed. Since the bedforms contributing to the roughness occur mainly at sub-grid model scales, the parameterization of k_s is a key element in a model's formulation. Because hitherto the bed roughness in natural settings has often been largely unknown, the common practice has been to assign a constant k_s value over the entire model area. However, the insights provided by acoustic multi-beam (MBES) instrumentation now give modellers a much clearer picture of the true and often highly variable nature of the seabed and set a challenge as to how best to incorporate a more realistic, spatially and temporally varying, description of the roughness in operational models. The fundamental question posed in this paper is whether a spatially/temporally variable k_s formulation provides a realistic description of the bedforms in a channel, while at the same time representing the tidal flow accurately.

The need for better representation of the bed roughness arises both in coastal areas where combined wave and current effects may be present and also in estuaries where salt-marshes and biological influences may be significant (Dalrymple et al., 2012). The starting point of the present study, involving

3

a tidal channel with roughness dominated by bedforms, is the empirical predictor of Van Rijn (2007) for non-cohesive sediments. For given local flow conditions this includes roughness contributions arising from sediment grains, small-scale ripples, mega-ripples and dunes. Van Rijn's (2007) formulation was tested in a Telemac model of the Dee Estuary, U.K., by Villaret et al. (2011, also 2012, 2013) and its use gave rise to enhanced bed roughness due mainly to dunes predicted in the main estuary channels. Importantly, the inclusion of this spatially/temporally varying k_s did not compromise the robustness of the numerical scheme.

The present paper provides a critical assessment of the use of variable k_s with reference to a natural tidal channel (Menai Strait, North Wales, U.K.) which exhibits strong reversing flows, a residual flow induced by the tides, a main tidal channel running between sand banks and over scour holes, and variable patterns of seabed roughness including dunes. The present numerical model, which is the most refined one of the Strait to date, has been developed using the Telemac Modelling System (Hervouet, 2007). The tidal flow is driven by free surface oscillations at its open ends that differ in amplitude and phase in a way that induces the pronounced residual flow. This tidal residual is used here as a diagnostic with which to assess the validity of various formulations for bed friction. The sediment transport is predicted for a seabed comprising an evolving mixture of three prescribed sand sizes overlying a layer of immobile material. The predicted k_s is fed back into the flow module, giving rise to flow-bed interaction throughout the simulation. The analysis is focused on both idealized spring-neap (SN) tidal cycles and also semi-diurnal (M_2) tides alone. In each case the roughness is computed online using Van Rijn's (2007) formulation for k_s, to which is added a new 'history effect' governing the temporal development of the dunes. The results are compared with outcomes determined using constant k_s values and the validity of the frictional representations is assessed with reference to the peak ebb and flood flow strengths and

4

also to the strength of the residual flow. The sediment transport rates in the channel are also estimated.

The specific questions posed here to assess the applicability of a spatially/temporally variable k_s include: What values of constant k_s give rise to the same bulk flows in the channel as predicted using variable k_s, and can the full SN-cycle be represented for simplicity by an 'equivalent' M_2 tide to reduce computational time? Does the mid-channel, maximum, roughness serve as a suitable calibration parameter to represent the channel as a whole or is a cross-channel average value more appropriate (Paarlberg et al., 2006, 2010)? Does the observed dune roughness in the channel agree with Van Rijn's (2007) predictor or does the fact that this predictor was determined for unidirectional river flows cause it to over-predict k_s for reversing tidal flows?

The organization of the paper is listed here. In Section 2 existing knowledge of the seabed roughness is assessed with emphasis on tidal environments. In Section 3 the study site (Menai Strait, N. Wales) is discussed highlighting the residual flow and earlier estimates of the seabed roughness. The Telemac model is described in Section 4 and here the procedures used to model the temporally/spatially variable k_s are explained. In Section 5 model outcomes are presented based on both constant and also temporally/spatially variable k_s for i) idealized spring-neap (SN) cycles and ii) semi-diurnal (M_2) tides alone. The sensitivity of the residual flow to these representations of k_s is assessed and an M_2 tide 'equivalent' to the full SN-cycle is identified. In Section 6 the predicted roughness k_s is compared with intra-tidal observations of the dunes, allowing an assessment of the roughness prediction scheme. The conclusions are presented in Section 7.

5

2. Seabed roughness

The presence of dunes on a mobile channel bed influences the hydraulic roughness, water levels and flow rates. The nature, mechanisms of formation and classification of dunes have been addressed by, e.g., Van Rijn (1993) and Fredsøe and Deigaard (1992). In steady flow in the absence of waves the profiles of dunes are roughly triangular, with a downstream leeside slope equal to the angle of repose above which a separation 'roller' occurs. The length of dunes in steady flow is strongly related to the water depth h, typically with λ_d = 7.3h, though with observed values of λ_d in the range 3h to 15h. Where bed-load dominates, the height η_d and length λ_d of dunes are related by $\lambda_d \approx 16\eta_d$. Due to the small bed slope of the upstream face, Fredsøe (1979) argued that formulae derived for sediment transport on a plane bed can still be used since the effect of gravity is small. Dune height in relation to water depth depends upon the transport stage and the median grain size d_{50} through d_{50}/h with dune form being complicated by three-dimensional effects in natural channels (Parsons et al., 2005). Where the suspended load becomes significant, λ_d increases in relation to η_d and bedform fields become less uniform (Venditti et al., 2015). Maximum values of η_d/h are about 0.2 in shallow flow of depth 1 m and about 0.1 in deeper flow of 10 m. The morphodynamic evolution of dunes in steady flow has been modelled recently using a 2-D approach by Doré et al. (2016).

Many studies of dunes have been carried out in rivers (Best, 2005) where the roughness of the main channel is sometimes used as a calibration parameter to match observed water levels. Several researchers have proposed methods to forecast river dune dimensions (see Paarlberg et al., 2006) with some attempts made to include the observed time-lag between dune dimensions and flow intensity (e.g. Allen, 1976; Fredsøe, 1979). However, Paarlberg et al. (2006) noted the inability of earlier models to predict the dune dimensions observed during river flood events. Such models have the further

6

drawback of determining the friction factor via the dune dimensions, rather than involving a direct formulation for the dune roughness k_{sd}.

In tidal flow in estuaries Dalrymple et al. (2012) suggested that dunes are somewhat smaller in scale than in steady flow, having $\lambda_d \approx 5h$ (where h is the depth corresponding to peak tidal flow) and with $\eta_d/h \approx 0.2$ as in steady flow. Van Rijn (1993) noted that the bedforms found most frequently in tidal currents and estuaries are mega-ripples and asymmetrical dunes, with η_d/h in the range 0.1 to 0.15, with smaller bedforms of height $\eta_d < 1$ m exhibiting asymmetry changes with the turn of the tidal currents. Zorndt et al. (2011) observed such dune heights and asymmetry effects in the tidal river Elbe. Dune lengths are smaller than those in steady river flow because the tidal period is not long enough for the generation of equilibrium values. Dunes generally occur in deeper wider tidal channels with bed material sizes larger than about 0.3mm. Van Rijn (1993) stated that tidal bedforms include:

i) mega-ripples in shallow channels with $d_{50} < 0.3$ mm ; $\eta_d = (0.05\text{-}0.1)h$; $\lambda_d = (0.5\text{-}2)h$

ii) sand dunes in deeper channels with $d_{50} = 0.3\text{-}0.6$ mm ; $\eta_d = (0.1\text{-}0.2)h$; $\lambda_d = (3\text{-}6)h$

However, the formulation of Van Rijn (2007) used later also includes dunes in finer sediment (see Fig. A1).

Flow resistance due to dunes arises from the combined effect of skin friction and form drag due to the expansion loss after each crest. This loss was estimated using Carnot's formula by Engelund (1978) and Fredsøe and Deigaard (1992), and the latter authors presented a flow resistance curve for dunes, based on similarity principles, that indicates the predominance of form drag at intermediate flow stages (see also Niemann et al., 2011).

7

For dunes defined as asymmetrical bedforms with length of about 7 times the water depth, Van Rijn (1993) proposed the following rule for the dune roughness:

$$k_{sd} = 1.1\gamma_d\eta_d\left(1 - e^{-25\eta_d/\lambda_d}\right) \qquad (1)$$

where γ_d is a form factor equal to 1 for angle-of-repose lee slopes and 0.7 for less steep slopes in field conditions. However, Van Rijn (1993) noted that a considerable reduction in the form roughness arises for dunes having mild leeside slopes above which separation is less important. This has been highlighted recently by a series of laboratory experiments carried out by Kwoll et al. (2016). With the horizontal length of the dune lee slope taken as λ_1 Van Rijn (1993, Fig. 6.2.8) indicated that, for values of λ_1/η_d greater than about 10 (i.e. gentle lee slopes), γ_d takes values smaller than 0.2. Li et al. (2006) suggested an improvement on Van Rijn's form factor based on FLUENT simulations which suggested an even more pronounced reduction in γ_d as λ_1/η_d increases. Lefebvre and Winter (2016) noted that angle-of-repose bedforms are rarely found in the field and highlighted the effect on k_{sd} of lee slope angle based on simulations made using Delft3D. However, the Reynolds-averaged model that they used did not resolve turbulence and intermittent flow structures, only permanent flow separation, resulting in a drastic reduction in γ_d between slope angles of 30° and 20°, with γ_d becoming < 0.01 at angles of < 15°. The severity of this reduction in γ_d is not easily reconcilable with the separation zones observed by Lefebvre et al. (2013) over lee side slopes of (10-20°). However, the detail of the bedform shape adopted has been shown recently to have influenced the model outcomes (Lefebvre et al., 2016). Observations of the velocity and turbulence fields were made above a 'sandwave' in a tidal estuary by Atkins et al. (1989). The field site was uncovered at low tide and then experienced flood-dominated flow with the depth reaching 4-5 m at high tide. The resulting bedforms in fine sand (d_{50} = 0.2 mm) had wavelengths of 15-20 m and heights of 0.8 m. In terms of Van Rijn's form factor the 'standard sandwave' had λ_1/η_d in the range 3.3-3.8 indicating a value of γ_d greater than 0.9 and, hence, large roughness k_{sd}. The

8

separating flow over these dunes was simulated by Johns et al. (1993), and a comparison with these data was carried out also by Li et al (2006).

Paarlberg et al. (2006, 2009) suggested a morphodynamic modelling approach for the prediction of dune dimensions involving cutting off the separation zone above the dune lee slope and computing only the steady flow above this (see also Van Duin et al., 2017). The shape of the zone was related to the dune dimensions, with flow separation occurring for leeside slopes exceeding 10° and with the flow then reattaching downstream at a typical distance of 5 to 6 times the dune height (cf. Fredsøe, 1982). The model was used to predict dune evolution, including asymmetry, and Paarlberg et al. (2010) later translated the estimated dune dimensions into roughness coefficients using Equation (1). The changing dune dimensions gave rise to hysteresis in k_{sd}, as observed during river flood events in which maximum dune heights occur a few days after peak discharge (Paarlberg et al., 2010). During such events the primary dunes cannot adapt instantaneously to the changing flow conditions. This can lead to a reduction in λ_d via the formation of secondary dunes, and also shorter and lower dunes (Wilbers and Ten Brinke, 2003), the composite effect of which can be included in the roughness formulation (Julien et al., 2002). Paarlberg et al. (2010) also noted the pronounced cross-channel changes in roughness caused by variations in grain size and current speed.

In reversing tidal flows these considerations remain, with the flow also being modulated through the SN-cycle. Bartholomä et al. (2004) made field observations of bedform behavior within individual ebb-flood tidal periods in the Grådyb channel, Denmark. While conditions at their study site appear somewhat similar to the channel considered in this paper, they reported that the bed was covered with very large compound dunes (length about 100 m, height 1.5 - 3 m) with superimposed medium-sized simple dunes. Only the latter features are present in the Menai Strait, apart from at its southwest end where some

9

larger features occur. Bartholomä et al. (2004) noted that dune heights showed considerable variation over the tidal period with the smaller superimposed dunes controlling the transport processes.

Paarlberg et al. (2010) noted that tidal dunes are more symmetrical than those in rivers, with the roughness description requiring adaptation on this account. A similar conclusion was reached by Lefebvre et al. (2011) who measured large compound bedforms through a tidal cycle in the Jade tidal channel, Germany. They found that published roughness predictors were unable to estimate not only the variations of the primary dune roughness but also tidally-induced changes in roughness for smaller secondary dunes. Lefebvre et al. (2013) made further roughness estimates from data obtained in the Knudedyb tidal inlet, Denmark. Here during the ebb tide they found that a permanent separation zone was established over the steep (10-20°) lee sides of ebb-oriented primary bedforms, whereas during the flood no separation was induced over the gentle (2°) lee slopes. In a modelling exercise using Delft3D, Lefebvre et al. (2014) investigated the presence and length of the flow separation zone in comparison with a predictive method (Paarlberg et al., 2009), with at least qualitative agreement achieved.

Allen (1976), among others, noted that dunes in river-dominated settings 'lagged behind the flow' and had a 'relaxation time' in excess of the time scale of change of the flow. This relaxation time, which can vary from hours to several days depending upon the scale of the system, is the time needed for the dunes to equilibrate with a changed flow. Van Rijn (1993) suggested adjustment rules for the evolution of η_d and λ_d involving a 'transition period' and Fredsøe (1979) explained the relaxation/transition time lag in terms of the expansion loss behind dune crests. Dalrymple et al. (2012) suggested further that profile asymmetry is strongly dependent on the size of a dune since the lag time increases approximately as the square of the dune size. They argued that in estuaries, while small simple dunes can reverse partially or completely during each half tidal cycle, large to very large compound dunes may

require months to do so and, thus, can provide an indication of the *residual* transport direction over such periods. Kostaschuk and Best (2005) noted that, in addition to the morphology of dunes in estuaries often lagging behind changes in SN-tides, changes in dune morphology also occur during the semi-diurnal tidal cycle. This effect was monitored in the Main Channel of the Fraser River estuary in water of depth 12-15 m with mean velocities of up to 2 m s^{-1}. Dune length did not change significantly during the 13-hour survey period, but changes did occur in dune height, steepness and leeside slope angle. Hysteresis loops indicated that η_d was in equilibrium with strong flows during the tidal cycle, but that λ_d was not, requiring longer to respond to the changing flow conditions.

The present study adopts Van Rijn's (2007) procedure to calculate k_s directly from the predicted sediment grain size, flow strength and water depth. This procedure, derived for steady flow, is accompanied by a new simple relaxation time, or 'history effect', designed to prevent unduly rapid variations in k_s during tidal cycles, but still allowing a slow modulation in k_s during the SN-cycle. Coleman et al. (2005) proposed a similar power law 'history effect' relating bedform wavelength and height to time with all parameters normalized by equilibrium values, starting from either plane bed or an initial bedform state. The roughness predicted in Section 5 is dominated by the dune component k_{sd}, which is critically assessed in Section 6 through observations made in the Menai Strait of dune dimensions, asymmetry and migration. This comparison highlights some of the differences noted above between dune occurrence in reversing tidal flows and more slowly varying river flows.

11
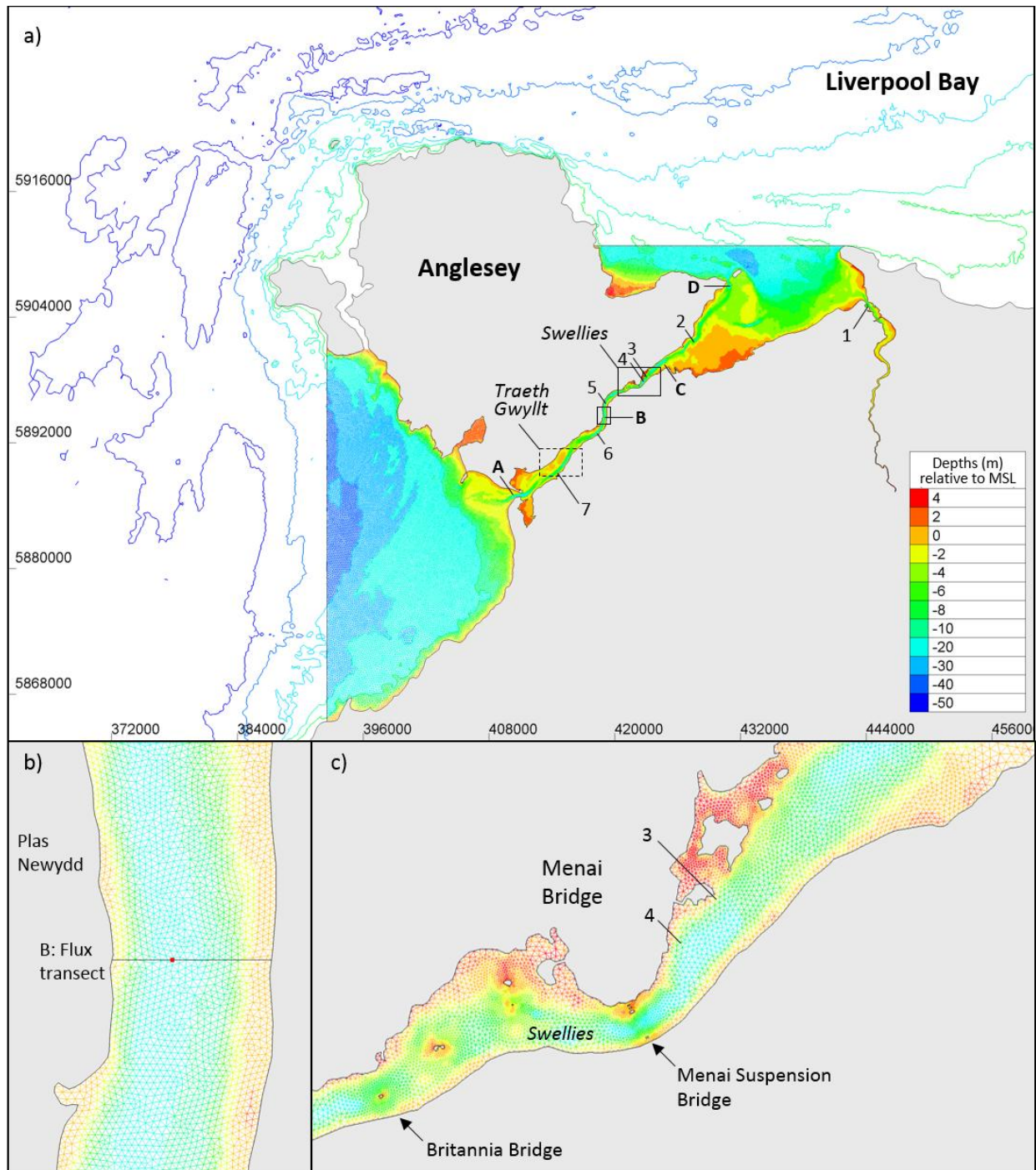
Figure 1. (a) Model domain extending between the northeast and southwest, open sea ends of the Menai Strait, North Wales. The model grid was mapped onto an assemblage of bathymetric data referenced here to Mean Sea Level (MSL). The model validation locations in Table 1 are shown as numbered points (1 to 7) while the locations of the tidal curves in Figure 2 at the open ends of the Strait are labelled A (Belan) and D (Puffin), with the mid-channel Flux transect labelled B (near Plas Newydd) and the end of the narrow section of the Strait labelled C (Bangor Pier). Traeth Gwyllt is indicated, where intra-tidal dune observations were made (Section 6 and Figure 11a). Inset (b) shows the model grid near the location of the 'Flux transect' used for the water flux calculations, with the mid-channel point

indicated (dot), and inset (c) shows the complex and shallow region around Menai Bridge and the Swellies.

3. Study site: Menai Strait, N. Wales

The Menai Strait, which separates the island of Anglesey from the mainland of Wales, has the geological and sedimentological setting discussed by Roberts et al. (2011). The Strait is approximately 20 km long with mean width of about 800 m between locations A Fort Belan and C Bangor Pier (Fig. 1). The volume of water within this length of the Strait is about 80 million m^3 at mean tidal level. Tidal ranges in the Strait are large, being of similar magnitude to the mean depth at some locations; the (M_2, S_2) tidal constituent amplitudes are, respectively, (1.6 m, 0.5 m) and (2.5 m, 0.75 m) at marked locations A and D in Fig. 1a at the open sea ends of the Strait. Tidal elevations at these locations are shown in Figure 2a. The instantaneous flow is driven by the larger tidal range at the northeast end of the Strait than at its southwest end, with a phase lag in elevation of about 40 minutes at the northeast end due to the time of travel of the tidal wave around Anglesey and into Liverpool Bay.
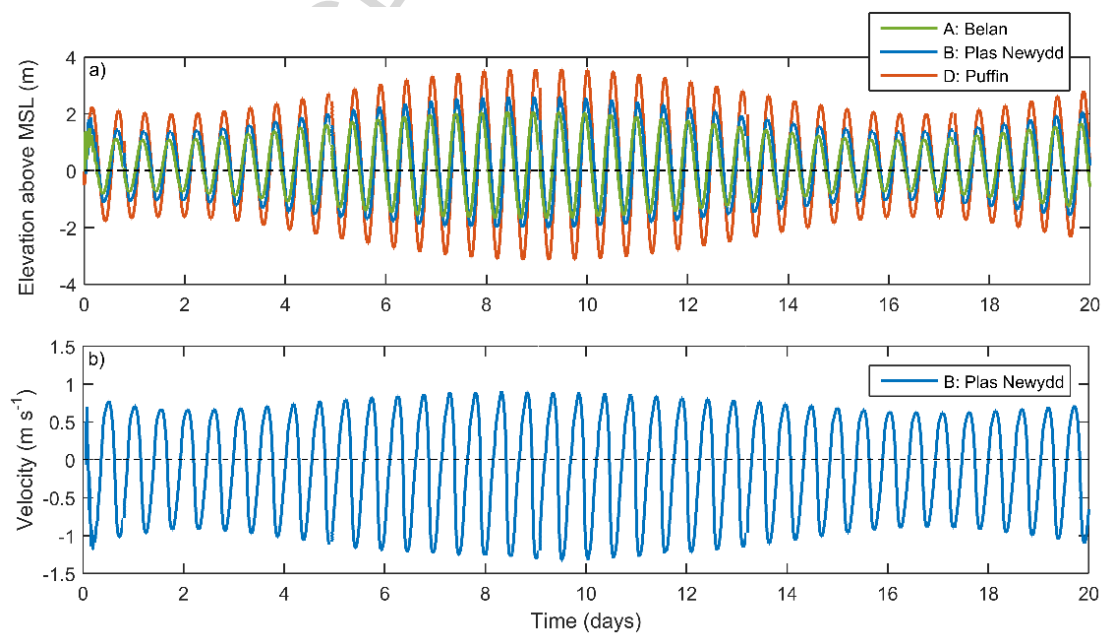

Figure 2. (a) Free water surface at the open sea ends of the Menai Strait (locations A and D in Figure 1, respectively) together with the elevation at the mid-channel location on the Flux transect (location B in

Figure 1). (b) Simulated depth-averaged velocities, at the mid-channel location (B), over a mean spring-neap tidal cycle. The results shown are for an idealised Neap-Spring-Neap cycle including M_2 and S_2 tidal constituents only. Following some irregularities in the initial cycle, a regular SN-cycle is simulated. Tidal constituent periods: M_2: 12 hrs 25.23 min; S_2: 12 hrs.

The tidal dynamics in the Strait are controlled by the shallow, central area of the Swellies (Fig. 1c), where the minimum flow cross-sectional area is located. Here, in contrast to the rest of the Strait, relatively large along-channel variations in tidal range and phase occur over a short distance. When high tide occurs in the Swellies, the flow towards the southwest is at its strongest, augmented by the reduced frictional resistance occurring for the deeper flow; in contrast at low tide, the frictional resistance is enhanced giving rise to a substantially weaker, shallow flow towards the northeast. The net effect is a residual flow towards the southwest with magnitude modulated by the stage of the SN-cycle. Early observations of the flow showed maximum instantaneous velocities of about 0.8 m s^{-1} towards the northeast and 1.5 m s^{-1} towards the southwest (Harvey, 1968), with a mean velocity of about 0.11 m s^{-1} occurring towards the southwest in conditions involving light winds.

Harvey (1968) took account of intra-tidal elevations in estimating water fluxes at four sections across the Strait and determined a southwesterly residual flow of magnitude up to 38 million m^3 in a 12½ hour period. Although Harvey (1968) did not fully identify the SN-tidal variation, his data obtained for the highest and lowest tidal ranges suggested a variation in the residual flow rates over a 12½ hour period from about 29 to 38 million m^3, corresponding to about 644 to 844 m^3 s^{-1}. Since Harvey (1968) took no account of cross-channel variation in velocity, his residual flow calculations based on mid-channel velocity observations were probably overestimated (see Section 5.2). Nevertheless his values corresponded to a significant proportion (~1/3) of the total volume of water within the Strait and suggested that the system has a flushing time of 2 to 3 days. Fresh water inflow into the Strait has been estimated as less than 0.5 million m^3 during a semi-diurnal cycle and is therefore unimportant. Harvey

14

(1968) noted, however, that variations in the southerly wind component were likely to bring about variations in the residual flow.

Simpson et al. (1971) investigated the effects of wind stress and tidal range on the residual flow using electromagnetic measurements made at a central transect. Their estimate of the net water transport over a spring tidal cycle was 48×10^6 m^3 in a 12½ hour period, which is somewhat larger than Harvey's (1968) value. The component of wind stress acting along the Strait was shown to augment the residual flow when from the northwest and to reduce, or even reverse it, when from the southwest. Regression analysis over a 4-month period suggested, for conditions of negligible wind stress, that the residual transport was in satisfactory agreement with Harvey's (1968) estimate. In the absence of wind, Simpson et al. (1971) estimated the residual flow to be about 800 m^3 s^{-1} at mean springs and 330 m^3 s^{-1} at neaps.

Observations of the along-channel water surface slope were made in a central part of the Strait by Campbell et al. (1998) to explore the dynamical balance and deduce the seabed drag coefficient C_D (bed shear stress $\tau_b = \rho C_D U^2$, ρ = water density, U = depth-mean velocity). The water column was shown to be vertically homogeneous, with horizontal density gradients too weak to affect the dynamics. For two periods of observation, the total transport of water, calculated from the cross-sectional area and the sectionally-averaged velocity, was respectively 26 and 30 million m^3 every 12.42 hours (or 578 and 667 m^3 s^{-1}), the latter value being for a period with stronger currents. The corresponding values of C_D determined along the centre-line of the Strait were 0.0088 and 0.0084, both values much larger than normally used (~0.0025) in shelf-sea applications. Assuming a log-velocity profile over the full water column and with the observed depths in mid-channel in the range 13m to 17 m, the roughness k_s implied by Campbell et al. (1998) varies from 1.8 to 2.6 m, which is unexpectedly large for flow in a sandy channel.

15

Further measurements of velocity and turbulence were made by Rippeth et al. (2002) over spring and neap tidal cycles at a closely adjacent site to that of Campbell et al. (1998) again in water of mean depth 15 m. The 'variance method' was used to extract the bed shear stress from ADCP turbulence data yielding a much lower value of $C_D = 2.6 \pm 0.2 \times 10^{-3}$. Due to uncertainties in their stress estimates, the authors suggested that these values could be increased by $\sim$11% making $C_D \sim 0.0029$, corresponding to $k_s = 0.10$ m based on an assumed logarithmic profile over the full depth. In contrast, estimates of the friction velocity u_* ($\tau_b = \rho u_*^2$) from the log-profile method produced larger values of the stress and, by implication, larger values of C_D. These C_D values were smaller on ebb (0.0032) than flood (0.0042), and smaller on neaps (0.0034) than springs (0.0040) (corresponding to k_s values of 0.14 m, 0.35 m, 0.17 m and 0.30 m, respectively). Rippeth et al. (2002) suggested that the difference between the estimates from the variance and log-profile methods might arise from the variance method measuring only the skin frictional drag while the log-profile also incorporates contributions due to larger scale form drag. However this explanation would only have force if the bed features were of relatively short wavelength in relation to the height range over which the log-fitting was carried out and the authors did not comment on the bed type and size on site. The smaller C_D values on the ebb than the flood could have been caused by the stronger ebb (southwesterly) flow generating dunes with asymmetrical profiles (steep face downstream). The weaker flooding (northeasterly) flow might then have experienced these features as an enhanced roughness (larger C_D). The observed SN-variation might indicate greater dune size on springs. All of these conjectures are assessed later.

Further consideration was given to the drag coefficient C_D through a 'tide-watch' (George, 2006). This was carried out over a semi-diurnal, mean spring tide at nine locations, and the outcomes were used to evaluate C_D for a series of reaches along the Strait. For the reach considered by Campbell et al. (1998)

and Rippeth et al. (2002), George (2006) obtained C_D = 0.0075. However, in a subsequent modelling study, George (2007) used the tide-watch data to suggest that a spatially varying C_D gave a reasonable fit between the modelled and measured data with:

C_D = 0.0035 southwest of the Swellies; 0.0050 in the Swellies; and 0.0020 northeast of the Swellies.

George (2006) noted the distorted nature of tidal curves southwest of the Swellies, where the tide falls approximately linearly for the first 2½ hours after high water and then rather faster. This behavior was attributed by Bowers et al. (2013) to a seiche that can produce a point of inflection in the tidal curve or a double high water.

4. Model implementation with bed roughness feedback

4.1 Telemac model – Implementation and validation

The simulations were carried out with the Telemac system (mainly v6p3, but also v7p1), based on finite-element algorithms, which allows complex coastal areas to be represented on an unstructured numerical grid (Hervouet, 2007; Villaret et al., 2013). The depth-averaged hydrodynamic module Telemac2D, which simulates the tidal flow in the Strait, was coupled with the morphodynamic module Sisyphe, which calculates sediment transport rates decomposed into bed load and suspended load. A key feature of the present implementation was the prediction by Sisyphe of the changing roughness k_s due to the combined effects of sand grains, small-scale ripples, mega-ripples and dunes. The details of the bed roughness scheme, which were outlined by Villaret et al. (2011), are summarised in Section 4.2 and Appendix A, together with the new 'history effect' applied to the dune roughness component k_{sd}.

The model domain includes the Menai Strait and coastal areas at both its northeast and southwest ends (Fig. 1). The unstructured grid comprising 131,800 computational nodes was created using the

17

BlueKenue™ grid generation software (Canadian Hydraulics Centre, 2011). The grid has variable resolution, from fine (~20 m) in the central channel of the Strait (Fig. 1b) to coarse (up to 500 m) elsewhere. This grid was mapped onto an assemblage of bathymetric data comprising: (1) multi-beam (MBES) data of the channel below mean low water springs, at high horizontal resolution (~5 m), collected during 2012; (2) LiDAR data of terrestrial and intertidal areas above the level of low water springs, at high horizontal resolution (2 m), collected during 2013; and (3) Admiralty bathymetric data of the offshore regions at either end of the Strait (interpolated onto a 200 m horizontal resolution grid). The amalgamated bathymetric mesh (Fig. 1) represents a significant improvement on grids used in previous studies. The model time-step was 2.5 s, and the model output was stored every 10 min (600 s).

Table 1. Model validation within the Menai Strait at locations shown in Figure 1. *H* = tidal amplitude (m), *g* = phase (degrees).

Tidal Gauge Station	M_2				S_2				N_2			
	Observed		Modelled		Observed		Modelled		Observed		Modelled	
	H	*g*	*H*	*g*	*H*	*g*	*H*	*g*	*H*	*g*	*H*	*g*
1 Conwy	2.43	319	2.43	310	0.67	008	0.67	349	0.35	293	0.35	289
2 Beaumaris	2.54	312	2.45	322	0.75	350	0.74	002	0.50	282	0.42	302
3 Ynys Faelog	2.49	306	2.33	312	0.93	331	0.69	352	0.38	292	0.38	294
4 Menai Bridge	2.32	316	2.26	322	0.75	357	0.68	002	0.43	295	0.39	303
5 Plas Newydd	1.81	299	1.80	302	0.69	342	0.62	341	0.36	280	0.33	283
6 Felinheli	1.71	302	1.73	312	0.52	339	0.55	349	0.36	277	0.32	289
7 Caernarfon	1.61	292	1.55	292	0.53	332	0.49	326	0.35	269	0.28	273

A baseline validation was performed using Telemac2D alone to check that the model could reproduce the tidal dynamics. The model was forced at each open boundary (i.e. at the ends of the Strait) by the five principal tidal constituents: semi-diurnal lunar (M_2) and solar (S_2), together with N_2, K_1, and O_1, all obtained from a regional-scale model of the Irish Sea (Lewis et al., 2015). The seabed friction was represented by a constant roughness (k_s = 0.32 m, a value determined from earlier work). The simulation was run for a period of two SN-cycles (i.e. 29.5 days), following a 24-hour model spin-up period. The model was then assessed by performing tidal analysis on the surface elevation time series

at several locations (Fig. 1a), and comparing the results to known amplitudes and phases of the primary constituents (M_2, S_2 and N_2). Additional measurements of surface elevation were collected for this purpose at locations 3 and 5 within the Strait. Comparing observed values and model output for the 7 locations (see Table 1), root mean square differences in amplitude and phase were 0.07 m and 7° for M_2, 0.10 m and 12° for S_2, and 0.05 m and 9° for N_2, respectively, each of which was deemed satisfactory. The comparison made at a location close to the water 'Flux transect' (Fig. 1b) provided important information, with data-model discrepancies here of only a few centimeters.

4.2 Sediment transport and bed roughness prediction

The sediment transport rate was calculated using the formulation of Bijker (1992), with seabed evolution then calculated by solving the Exner equation, including sloping bed effects (see Davies and Thorne, 2008; also Mendoza et al., 2017). For simplicity the suspension procedure available in Sisyphe was not utilized, i.e. advection-diffusion was not used for the suspended sediment. The transport procedures were implemented in the coupled model assuming a seabed composed (initially) of a representative upper layer of three sediment sizes (0.125, 0.25 & 0.5 mm) in the volumetric proportions 30%, 50% and 20%, respectively, overlying a layer of non-erodible cobbles of size 10 mm. The artifice of a coarse underlying layer is particularly important in the shallow region of the Swellies where strong currents would otherwise give rise to unrealistic bed erosion. The thickness of the initial, erodible, upper layer was chosen as 30% of the local water depth, subject to minimum and maximum assumed values of 0.5 m and 5 m, respectively, and with an initial erodible layer thickness of 1 m imposed in the Swellies. As a typical simulation proceeds, the sediment mixture in the upper layer is redistributed through differential transport of the component grain sizes and the cobbles can become exposed in places. The evolving sediment mix in the upper layer determines the mean grain diameter used in the

19

roughness prediction scheme which, in turn, influences the flow strength. The interactive formulation is therefore quite complex and the simulation time correspondingly lengthy.

A key part of the present coupled simulation involves the seabed roughness, which was predicted by the model, rather than being specified as a global value for the entire domain (cf. the validation in Section 4.1). In nature, the dimensions of bedforms vary spatially and with time, as a function of the flow field and sediment characteristics (Section 2). The time-varying total roughness k_s was calculated here at each grid node by Sisyphe and then used by Telemac2D. The total bed shear stress was partitioned in Sisyphe such that only the small-scale ripple roughness was used for local sand transport predictions. The feasibility of this method of feedback between the hydrodynamic and morphodynamic models was demonstrated previously in estuarine applications (e.g., Villaret et al. 2011), with the methodology appearing robust and without unstable feedbacks occurring between the mean flow and the bedforms.

The method of bed roughness prediction and the modelling methodology are presented in Appendix A. Van Rijn's (2007) empirically-based formulation for k_s is simply applied and offers a physically consistent approach to represent the sub-grid-scale processes; typical dunes having wavelength O (10 m) are here represented as 'roughness', rather than 'topography', the minimum local grid size being ~20 m. The formulation predicts the local bed roughness only and does not permit any lateral spreading of dunes along their crest lines, as tends to occur on site towards the shallower margins of the Menai Strait, i.e. no diffraction-like effect is modelled here.

The predicted bed roughness depends upon a single parameter, namely the mobility number, and includes contributions due to small-scale ripples (k_{sr}), mega-ripples (k_{smr}) and dunes (k_{sd}). The formulation does *not* involve the prediction of the dimensions (height and wavelength) of the respective

20

bedforms since Van Rijn argues that this is an unnecessary complication. Instead, direct estimates are made of the roughness components that are then used to calculate both the bed friction encountered locally by the mean flow and also the local sediment transport rate. Initially, k_{sr}, k_{smr} and k_{sd} are computed quasi-steadily, and are then combined into a total bed roughness $k_{s,TOT}$, taking no account of the 'history effects' that occur in reality in a tidal flow. The limitations of a simple quasi-steady approach were illustrated by McCann et al. (2011) who compared model results for k_s with observations of bedforms made in a shallow estuarine flow. The model results for k_s fluctuated strongly on a short tidal time scale, while the observations only exhibited smaller, damped, temporal variations. This suggests that, while a quasi-steady approach can illustrate the effects of spatial variation in k_s, it can misrepresent some potentially important aspects of roughness 'feedback' into the dynamics of the flow.

The aim of the new 'history effect' included to address these shortcomings is to inhibit the rate of bedform growth/destruction in a realistic manner. Only the dominant dune roughness component is adjusted here, though the same principle and methodology may be applicable also to mega-ripples. A time scale T_d for the growth/destruction of a simple dune (Section 2) is suggested as: $T_d \sim {d}/{U}$ where d (= d_{50}) is the sediment grain size and U the strength of the flow. So the larger are the grains the longer is T_d, and the larger is the velocity the shorter is T_d. The time of formation/destruction of fully-developed dunes can then be expressed via a calibration constant γ_s, as follows: $T_d = {d}/{U} \times \gamma_s$ s where γ_s is $O(10^8)$. This time scale T_d is assumed here to provide the simplest basis upon which to define a lag effect, or 'history effect', for dune growth or erosion. If at a particular grid location and model time step the quasi-steady approach to the calculation of k_{sd} implies a dune growth/destruction rate that is faster than that which can possibly be attained according to the time scale T_d, then the growth/destruction rate of the dunes is inhibited. The procedure is explained in Appendix A.

5. Model results

5.1 Hydrodynamic and sediment transport simulations

A central aim was to use the validated model to simulate the tidal flow across the Flux transect (see Fig. 1b), and hence to calculate the net water flow through the channel at this location. To this end, 20-day simulations were carried out to include a mean SN-tidal cycle (i.e., 14.75 days based only on the M_2 and S_2 tidal constituents). No wind or wave effects were included and k_s was predicted by the model. The tidal elevations at the ends of the Strait are shown in Fig. 2a, together with the resulting elevation at the middle of the Flux transect. This is somewhat larger in amplitude and almost in phase with the elevation the southwest end of the channel (location A). Fig. 1b shows the numerical grid in the vicinity of the Flux transect; here the grid resolution of nominally ~20 m can be seen in relation to the transect, together with the mid-channel point (red marker). The tidal range at this point is $\approx$ 4.7 m on springs and $\approx$ 2.5 m on neaps; the tidal range is significantly smaller on the southwest side of the Swellies than on the northeast side. A time series of depth-averaged velocity at the mid-channel point is shown in Fig. 2b. The peak spring (negative) ebb depth-averaged tidal velocities directed southwards are stronger (up to 1.35 m s^{-1}) than the (positive) flood velocities (up to 0.8 m s^{-1}) directed northwards. The peak neap currents are weaker, reaching 0.8 m s^{-1} during the ebb and 0.5 m s^{-1} during the flood. Strongest flows occur in the southerly direction because, at this stage of the tide, water depths are greatest due to the tidal forcing at the northeast open-sea boundary. Because of the consequent flow speeds at high and low water, there is a significant **net** flow through the channel from its northeast to its southwest end, i.e., southward across the Flux transect.

Based on the defined mixture of bed sediment sizes (Section 4.2), the predicted roughness k_s during spring tides (Fig. 3a) suggests the presence of dunes in mid-channel, with rather featureless beds

22

towards the shorelines, as observed. At the location of the Flux transect, the dunes achieve heights (assumed here to equal k_s, see Section 6) of about 0.6 m in the main channel, while towards the shores the roughness corresponds to small-scale sand ripples or featureless rough beds. These latter areas occur particularly in the shallower water towards the eastward end of the transect. The roughness k_s shows relatively little SN-variation once the dunes have become established; after 'growing' during the first couple of days, they are predicted to persist with only small modifications thereafter due to the imposed 'history effect' (Appendix A). The time series (Fig. 3b) of k_s at the mid-channel point shows both intra-tidal temporal changes and also a systematic, albeit small, SN-variation.
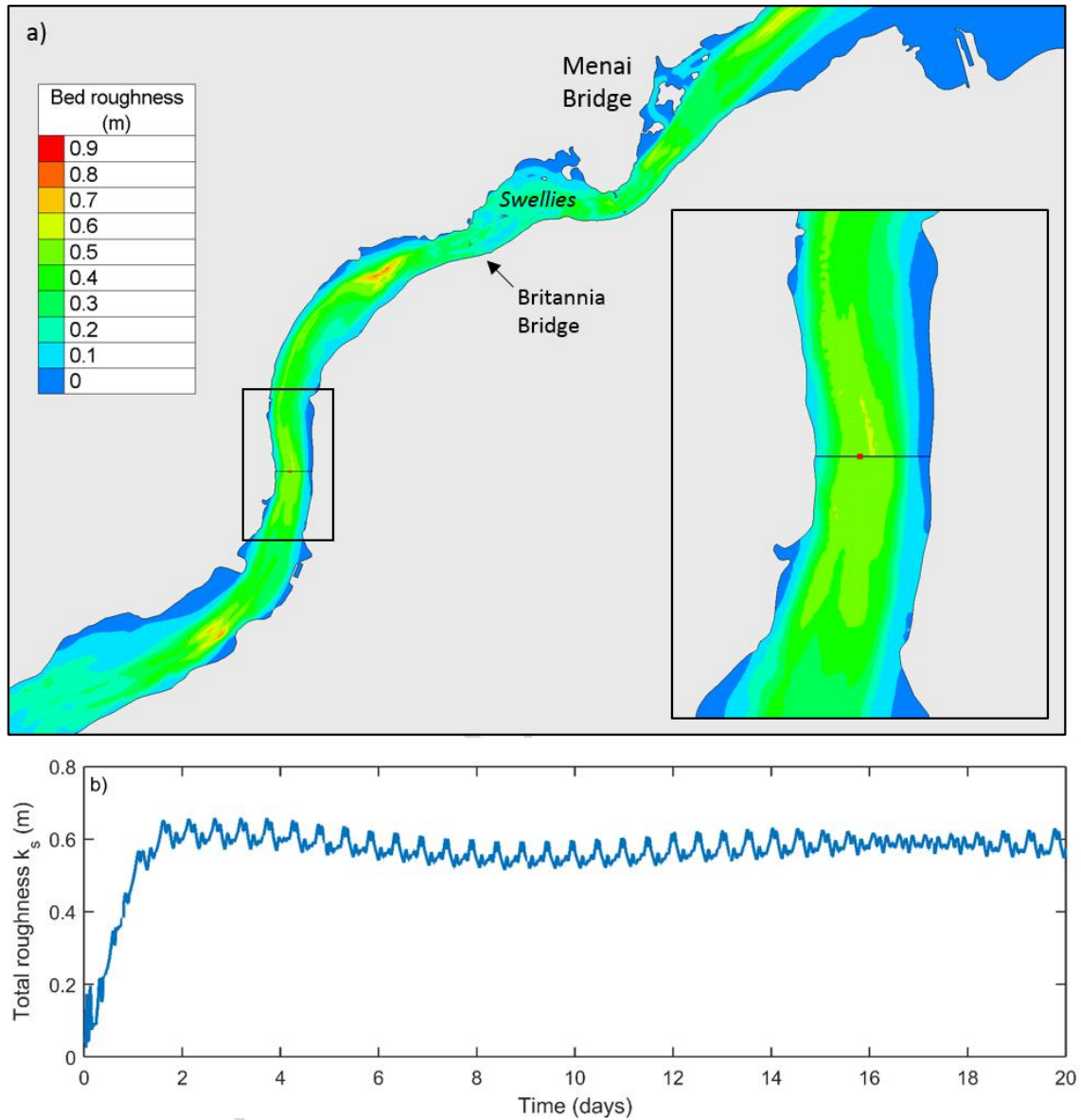
Figure 3. (a) Total bed roughness k_s (m) predicted within the Menai Strait during a peak spring tide, including the region of the Flux transect (highlighted in the inset, which also shows the mid-channel location as a dot); (b) variation of k_s (m) during 20-day simulation at the mid-channel point.

The mean sediment grain size varies in the surface (upper) bed layer during a simulation. After 20 days, coarser sediment (exposed cobbles from the non-erodible lower layer) is predicted to occur (Fig. 4) in the shallow water at the edges of the Strait with finer sediment in the main channel, as observed. This redistribution is probably enhanced by any localised wave effects at the margins of the channel. The

24

grain-size texture predicted for the surface layer is shown in more detail in the inset. Again, the finest

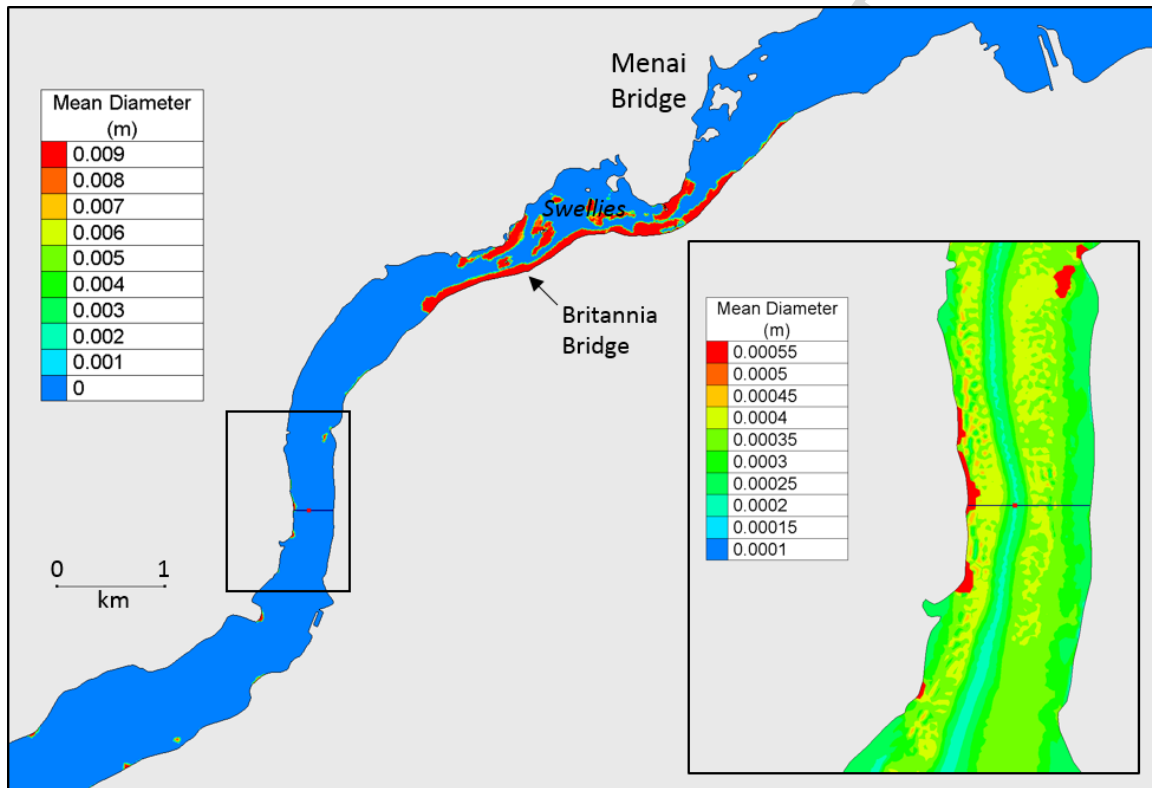sediment occurs in the main channel with a coarsening tendency on either side.

Figure 4. Mean sediment grain size (m) predicted after 20 days of sediment redistribution on the bed. The main map highlights the coarse cobble fraction which becomes exposed, particularly in the area of the Swellies, while the inset gives a more detailed view of the distribution of the sand sizes in the vicinity of the Flux transect, focusing on the smaller grain fractions.

Based on the 3-sediment mixture, Fig. 5a shows the predicted magnitude of the sediment transport rate

(in $m^2 \, s^{-1}$) at maximum spring tide with the flow towards the south giving rise to relatively large

transport rates in the centre of the channel. Towards the shorelines, little sediment movement is

predicted. In contrast, the transport to the north on spring tides is very small. At the mid-channel point,

the sediment transport (plotted in Fig. 5b as a scalar) is predominantly southwards (large peaks) with

only small intervening northward transport contributions (small peaks). The resulting net sediment flux

is southwards, and so its direction is the same as that of the residual flow discussed in Section 5.2.
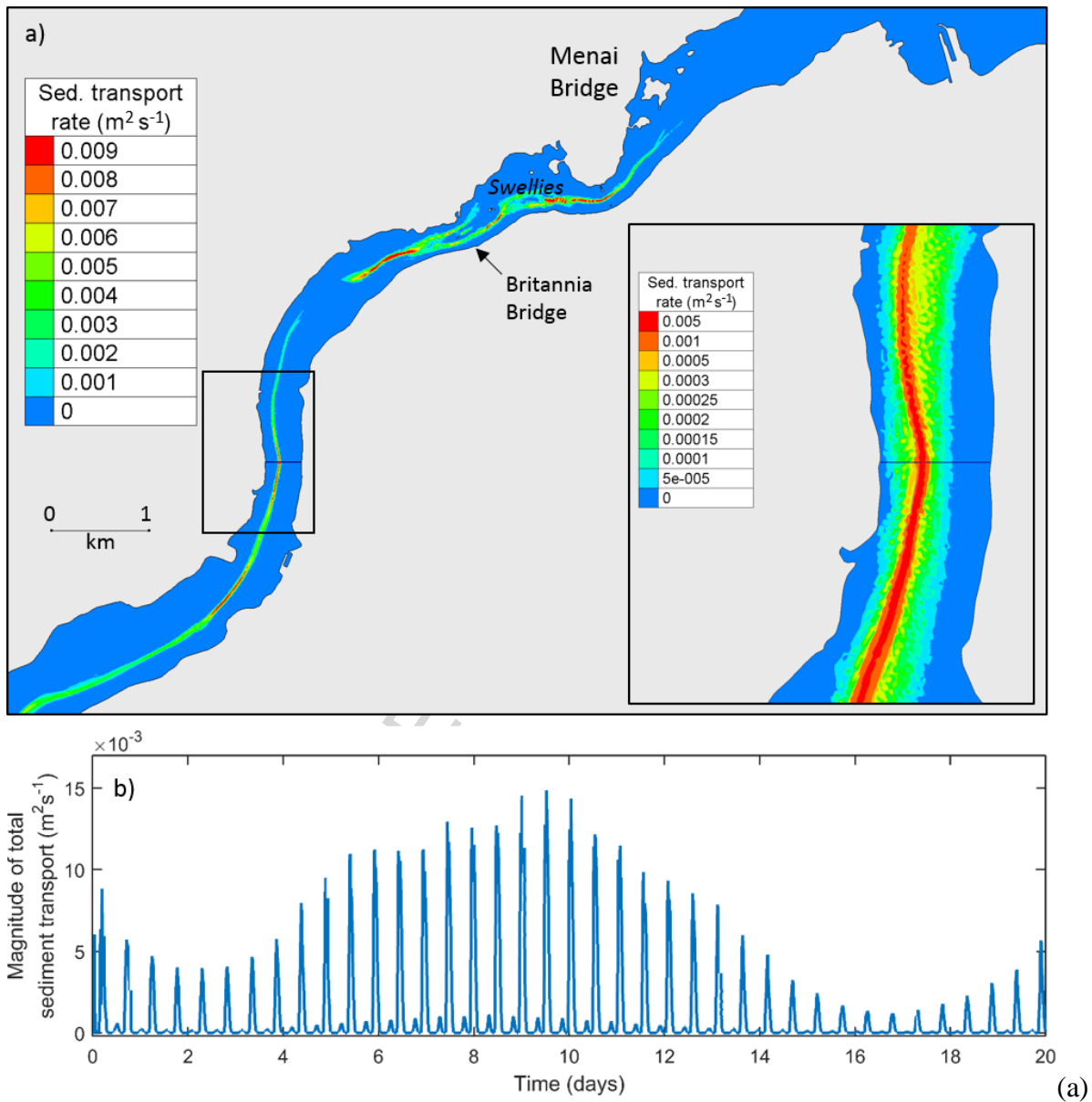
25

Figure 5. (a) Predicted total sediment transport rate ($m^2 s^{-1}$) when peak flow on spring tide is southward, with the region of the Flux transect highlighted in the inset; (b) sediment transport at the mid-channel point on the Flux transect, plotted as a scalar.

All of the results above are for a mean SN-cycle (M_2 and S_2 only). Variations around this typical mean pattern will occur in practice due to the presence of smaller tidal harmonics not included in the simulations.

26

5.2 Water flux results

The residual flow across the Flux transect is used here as a diagnostic to assess various bed roughness descriptions implemented in Telemac2D via Sisyphe. Firstly, an idealised SN-tidal cycle was simulated with i) predicted spatially/temporally varying k_s and ii) several fixed values of k_s (0.05, 0.15, 0.30 and 0.45 m) throughout the domain. Each run was carried out for a duration of 20 days allowing a spin-up period of about 2 semi-diurnal cycles for the flow and, where needed, about 3 cycles for the variable k_s, before commencing the averaging process to extract the residual flow. Secondly, an M_2-alone cycle was simulated to assess whether a simple 'equivalent M_2 tide' can be defined to represent aspects of the full SN-cycle in order to reduce computation time. To this end a series of M_2-alone runs was performed, again with i) varying k_s and ii) fixed values of k_s (0.05, 0.10, 0.20, 0.30, 0.40 and 0.50 m). The M_2-alone simulations were of duration 50 hours and were run for convenience with a tidal period of 12.5 h. In these runs the flow and bedforms became established on the same time scales as for the SN-cycle allowing flux averages to be obtained during the final 12.5 hours.

The instantaneous, north-south, v-component of velocity was calculated on the grid shown in Figure 1b and then interpolated in BlueKenue onto the west-east transect of length 365 m using a regular interval of 5 m. The predicted variable k_s across the transect at the end of the 50-hour M_2-alone simulation is shown in Figure 6. Peak values of $k_s \approx 0.6$ m occur in the main channel where dunes are predicted (cf. Fig. 3) with smaller values of k_s towards both shores. The effect of variable versus fixed k_s on the v-
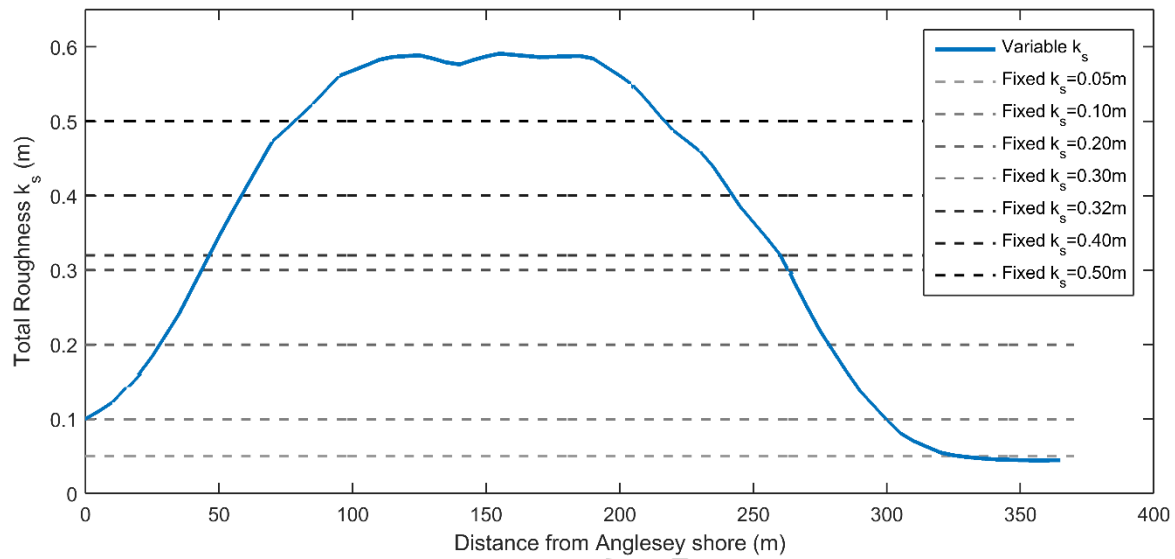
Figure 6. Predicted variable bed roughness k_s after 50 hours of the simulation with M_2-alone. The k_s values were interpolated along the Flux transect using a 5 m interval. The spatially invariant values of k_s used in the M_2-alone simulations are indicated by the dashed lines.

velocities across the transect is illustrated in Fig. 7a. Fixed k_s gives rise to smaller flow speeds near both shores where the variable k_s tends to be smaller. In contrast in the main channel the dune roughness gives rise to a flow speed that falls between the values obtained with fixed values of k_s = 0.05 m and 0.5 m. With low constant k_s (light dashed line in Fig. 7a for which the value imposed is equal to about the minimum value predicted along the transect), velocities are greater in mid-channel than for variable k_s. With high constant k_s (dark dashed line in Fig. 7a) the water flux is reduced as expected, with lower flow speeds found in mid-channel than for variable k_s, even though k_s = 0.5 m is lower than the predicted k_s value in mid-channel. Close to the shore, flow speed variations arise from overall water flux constraints, with even a flow reversal predicted on the eastern shore for small constant k_s values, which is not due to wetting and drying effects according to Fig. 7b. The use of a fixed k_s necessarily provides overall qualitative agreement with the variable k_s solution. However, the differences in the predicted velocities are actually quite large, and therefore capable of triggering potentially different morphodynamic outcomes. It should be noted that during the M_2-alone simulations the bed evolution predicted by

28

Sisyphe was fed back into Telemac2D. However, the water depth changes on this account were too small to have affected the results shown in Fig. 7a significantly.
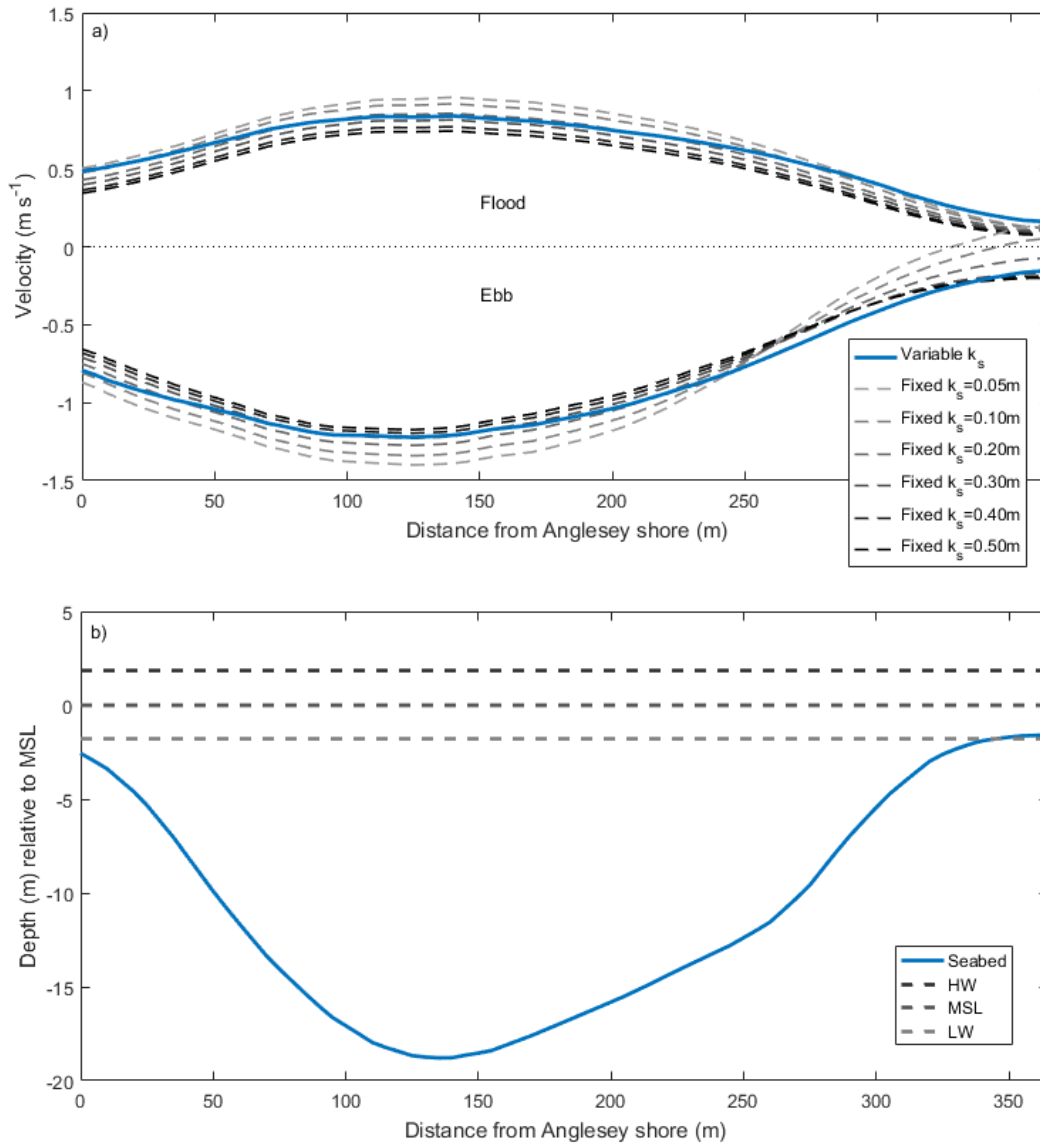

Figure 7. (a) Peak northward (positive) and southward (negative) flows across the Flux transect during the final cycle of the M₂-alone simulation. The v-velocity profiles obtained with variable k_s are shown as full lines in the respective directions. The results using fixed k_s values are shown by the dashed curves which correspond to those in Figure 6. (b) Water depth (m) across the Flux transect relative to Mean Sea

Level (MSL) together with High Water (HW) and Low Water (LW) elevations during the M_2 cycle (dashed lines).

Simpson et al. (1971) estimated that the mean (cross-sectionally averaged) velocity in spring and neap conditions at a neighbouring transect across the Strait was approximately 0.87 times the maximum, mid-stream, depth-averaged current velocity. This calculation was repeated here using the model results for variable k_s obtained at the Flux transect. For tidal phases corresponding to peak velocity northward and southward the quotients relating the mean and peak depth-averaged velocities were 0.86 and 0.81 respectively, i.e. somewhat smaller than Simpson et al.'s (1971) estimate. The magnitude of the quotient varies in time around these representative values which were obtained during rising and falling tides respectively.
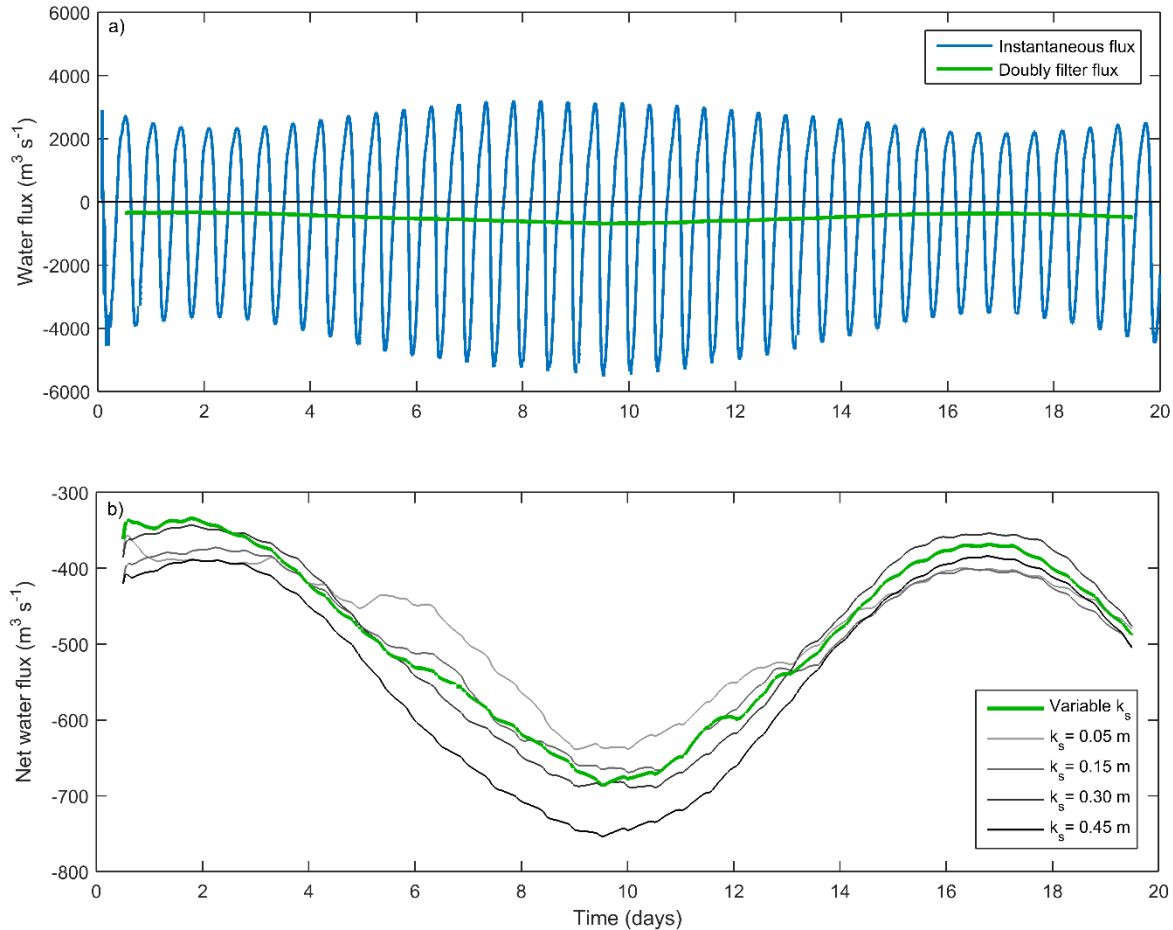
Figure 8. (a) Predicted instantaneous water flow though the Flux transect during a SN-cycle with variable roughness k_s. Positive values of flux are northward. Double box-car filtering of the instantaneous fluxes gives rise to the averaged residual outcome. (b) The slowly-changing residual water flux through the SN-cycle is shown in more detail, together with the corresponding fluxes for four fixed values of k_s.

The water fluxes were determined in BlueKenue by forming the product of the v-component of velocity and the instantaneous local water depth h at each point across the Flux transect. These 74 values of h*v at 5 m spacing were integrated to give the instantaneous water flux every 10 minutes. The results for the SN-cycle with variable k_s are shown in Fig. 8a. Following an initial model spin-up period, the water flux shows a predominant M_2 oscillation modulated by S_2 with larger peak fluxes southward and smaller peak fluxes northward. The southerly (negative) residual was extracted through the use of a simple box-

31

car filter with duration roughly equal to that of the M_2 tidal cycle. Since the model output was only stored every 10 minutes, it was found that double use of this filter was required to remove an M_2 oscillation in the residual still present on first use of the filter due to the slight mismatch between the box-car duration and the M_2 period. Double use of the filter yielded the outcome in Figs. 8a and 8b which shows a southerly residual flow that roughly doubles in strength from neap to spring tide from 334 $m^3\,s^{-1}$ to 686 $m^3\,s^{-1}$ (see Table 2). This agrees quite well with the neap-to-spring variation of 330 to 800 $m^3\,s^{-1}$ estimated by Simpson et al. (1971) and is consistent with the subsequent flux estimate made by Campbell et al. (1998). The overall mean flux was obtained by applying a further 14-day box-car filter, which yields a settled residual after about 14 days until the end of the simulation at 20 days. The mean flux was thus estimated for the SN-cycle with variable k_s as $-525\ m^3\,s^{-1}$.

Table 2. Residual flow in the Menai Strait calculated for the SN-cycle using variable predicted k_s and constant fixed k_s values. The negative values signify flow towards the southwest end of the Strait, with larger flow magnitudes occurring on springs than neaps. The average of the spring and neap values is shown in brackets for comparison with the overall SN-mean value.

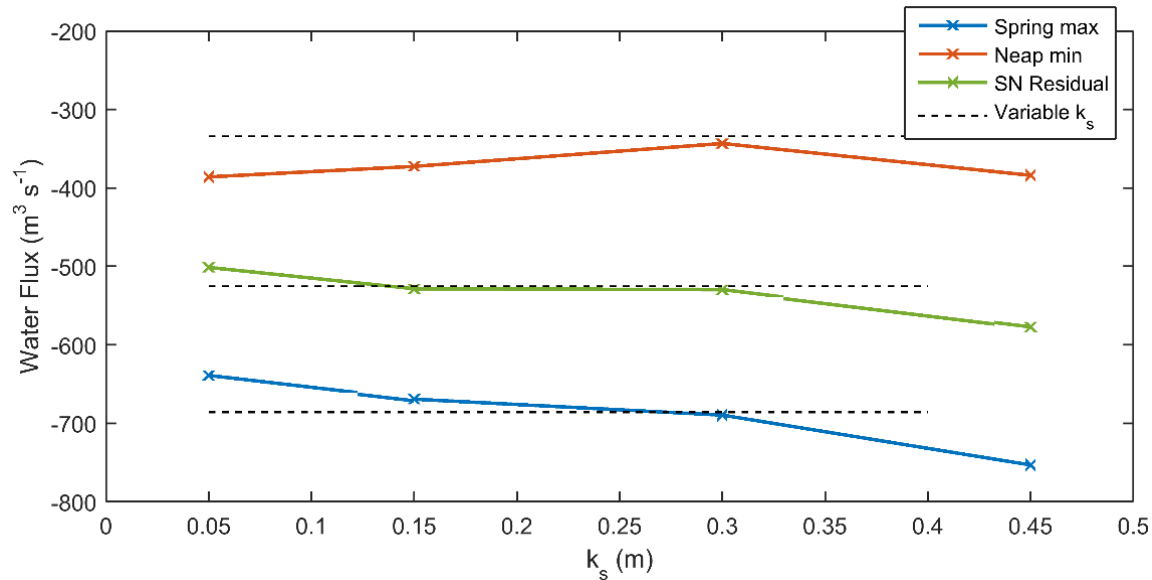| Residual ($m^3\,s^{-1}$)	Variable k_s	k_s = 0.05 m	k_s = 0.15 m	k_s = 0.30 m	k_s = 0.45 m
Spring max	-685.9	-638.9	-669.2	-689.5	-753.1
Neap min	-334.3	-386.0	-372.6	-343.4	-384.0
SN mean (Av. max & min)	-525.4 (-510.1)	-501.3 (-512.5)	-528.5 (-520.9)	-529.6 (-516.5)	-577.1 (-568.6)

Figure 9. Residual water fluxes at the Flux transect for the SN-cycle calculated using variable k_s (dashed lines) and various fixed constant k_s values. The results shown are for the spring, neap and overall SN-mean residual water fluxes.

Equivalent results for the SN-cycle obtained with the various fixed k_s values are shown in Fig. 8b from which the results shown in Fig. 9 have been extracted to highlight the residual fluxes at peak springs and neaps together with the overall SN-mean flux. The spring tide residual velocity increases significantly in magnitude as the constant k_s value increases. In contrast, the magnitude of the neap tide residual, while varying over a smaller range as expected, decreases to a minimum when $k_s = 0.3$ m. The overall SN-mean residual was calculated as described above and is shown in Table 2 in comparison with the average of the spring and neap residual values. While the (negative) SN-mean value increases in magnitude as the constant k_s value increases, it remains roughly constant in the centre of the k_s range shown. In order to recover the variable roughness outcomes (dashed lines) using a fixed value of k_s, the required values are approximately:

Spring residual: **k_s ~ 0.27 m**   Neap residual: **k_s ~ 0.30 m**   Overall SN residual **k_s ~ 0.20-0.30 m**
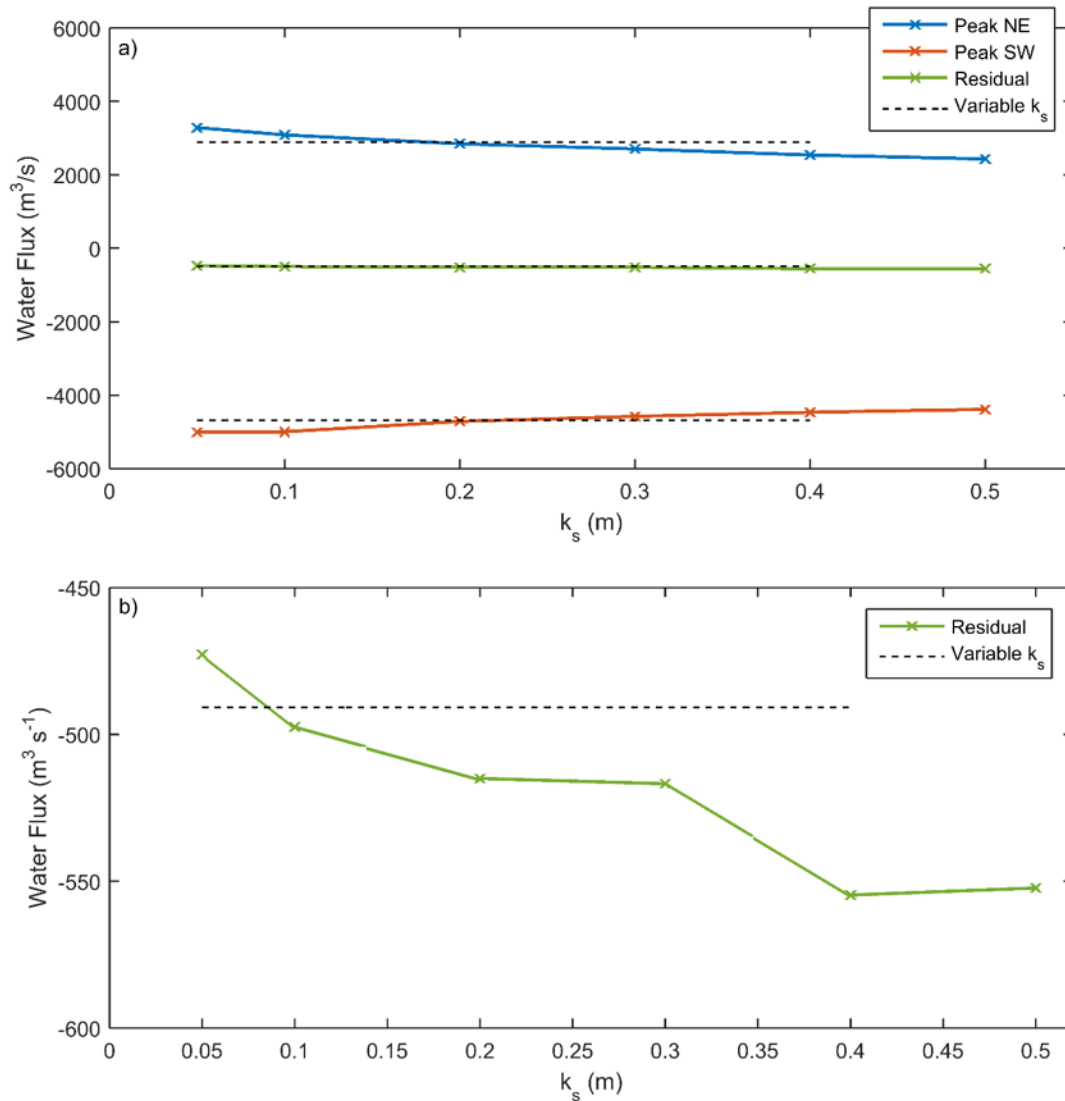
33

Figure 10. (a) Peak instantaneous and residual water fluxes at the Flux transect for the M_2-cycle calculated using variable k_s (dashed lines) and various fixed constant k_s values. The results shown are for the northward and southward peak instantaneous fluxes, together with the M_2-mean residual water flux. (b) The residual flux is shown in detail.

Each of these values is significantly smaller than the mid-channel values of roughness shown earlier, suggesting that use of a mid-channel value (Fig. 6) as the overall fixed k_s value would understate peak flow rates, while overstating the residual flow. The values of k_s themselves are in reasonable agreement with those obtained by Rippeth et al. (2002) based on the logarithmic profile method, but are substantially larger than their estimate determined by the turbulence 'variance method' (see Section 3).

For the 50-hour M_2-alone runs the residual flow computations involved a similar process of double-filtering to that used for the SN-cycle. With spatially-temporally varying k_s the residual flux for M_2-alone was -491 m^3 s^{-1}, which is about 7% smaller in magnitude than the value for the SN-cycle. Again M_2-alone results were obtained for comparison using a range of fixed constant k_s values. For variable k_s the peak northward and southward fluxes across the transect were 2900 m^3 s^{-1} and -4682 m^3 s^{-1}, reflecting the dominance of the flow towards the southwest. Fig. 10a shows a comparison between these values and the results obtained for M_2-alone with fixed constant k_s values. Both the northward and southward peak fluxes decrease in magnitude significantly as k_s increases. In contrast, the relatively small residual velocity, shown in detail in Fig. 10b, increases in magnitude as k_s increases, as found in Figs. 8b and 9 for the SN-cycle. In order to recover the variable roughness outcomes (dashed lines), the required fixed values of k_s are approximately:

Peak northeast flow: **k_s ~ 0.17 m**   Peak southwest flow: **k_s ~ 0.25 m**   Residual flow **k_s ~ 0.085 m**

Again, each value is significantly smaller than the mid-channel values of dune roughness shown in Fig. 6.

5.3 'Equivalent' M_2 tide and overall predictions of k_s

Comparing the outcomes for the residual flow in the case of variable k_s (Table 2), the overall mean values for the SN-cycle (-525.4 m^3 s^{-1}) and M_2-alone (-490.8 m^3 s^{-1}) differ by about 7% due probably to the enhanced contribution to the flux from spring tides compared with neaps. In order to match the SN-cycle value, an enhanced 'equivalent' M_2-tide can be defined. This has been determined by re-running the M_2-alone case with variable roughness using an enhanced M_2-amplitude. In particular, the time-varying tidal heights have been rescaled uniformly at both model open sea boundaries from which it has been found that the SN-residual can be recovered by an 'equivalent M_2' tide of amplitude enhanced by 7.3%. It would seem from this that the residual flow in the Strait is related approximately linearly to the

M_2 amplitude. This enhancement is qualitatively similar to the 'morphological tide' determined by Latteux (1995) as the best single equivalent tide to represent sediment transport during a full SN-cycle. This morphological tide lies between mean and spring tidal conditions, due to the strong nonlinear relationship between sediment transport and flow velocity that causes the bed morphology to be related more to spring tides, hence requiring an enhancement of the mean M_2 amplitude. Similar considerations evidently apply in the definition of the present 'equivalent M_2' tide.

Finally, it may be noted that, if the predicted variable k_s values are spatially averaged within the Menai Strait, between locations A and C (Fig. 1a), the value obtained at the end (after 50 hrs) of the M_2 alone simulation is $k_s \approx 0.15$ m. This is about a quarter of the peak value of k_s typically resulting from the dunes in mid-channel (Fig. 3, 6). The spatially-averaged value for the entire model domain is about $k_s \approx 0.20$ m. These spatially-averaged k_s values are somewhat smaller than the range of k_s values of 0.2-0.3 m which provides a reasonable representation of both the instantaneous peak fluxes and also the residual flux for M_2 alone. This points to the dynamics in the Strait being more influenced by the larger roughness encountered by the stronger flow in mid-channel, than by the shallower areas where smaller k_s values are predicted. In summary, the effective roughness of the seabed in the Menai Strait is less than 50% of the maximum local roughness due to the dunes in mid-channel, but more than the spatially mean predicted roughness in the Strait as a whole by about 50%.

6. Discussion : k_s observed versus predicted

As illustrated in Fig. 3, Van Rijn's (2007) predictions for k_s are dominated in mid-channel by the contribution from dunes, with smaller contributions arising from mega-ripples and small-scale ripples (Fig. A1). The predicted overall roughness, augmented by the new 'history effect', gives rise to realistic

36

water fluxes. However while dunes are predicted to form for the velocities, grain sizes and water depths occurring in the Menai Strait, a question arises as to whether these dunes formed in tidal flow achieve the wavelengths and heights that would occur on an extended timescale in an equivalent riverine setting involving steady flow for which Van Rijn's (2007) formulation may be most appropriate. In particular, is Van Rijn's (2007) suggestion (see Appendix A, Section A1) that the contribution k_{sd} of dunes is 'roughly on the order of half the bedform height' borne out by observations of the dunes on site?

Observations of dunes in the Menai Strait were made by McAleese (2012) at a mid-channel location in the vicinity of Traeth Gwyllt (Fig. 1a), where the water depth, bed sediment size and flow conditions were closely similar to those considered in Section 5. The main aim of these observations was to assess whether any significant variations occurred in dune length, height or asymmetry on intra-tidal timescales. Multibeam echo sounder data were collected on 19th April 2012 by Bangor University. The system was successful in measuring changes in dune heights of the order of 0.02 to 0.04 m and the overall vertical and horizontal resolution achieved was ± 0.02 m, with sampling carried out at a nominal horizontal interval along the bed profiles of 0.01 m. Four along-channel profiles (P1-P4) (Fig. 11a) of length 110-120m were interrogated at nominally 40-minute intervals for a period of 5.5 hours on a falling ebb tidal flow towards the southwest with water depths decreasing from about 15 m to 11 m.

Table 3. Dune observations made by McAleese (2012) in the vicinity of Traeth Gwyllt (η_d = dune height, λ_d = dune length, λ_1 = horizontal length of dune lee slope, γ_d = form factor)

Profile	η_d (m) mean	λ_d (m) mean	λ_1 (m) initial	λ_1 (m) final	λ_1/η_d initial	λ_1/η_d final	λ_1/η_d mean	γ_d initial	γ_d final	γ_d mean
P1	0.47	7.4	4.4	3.0	9.4	6.3	7.8	0.29	0.70	0.47
P2	0.32	6.1	3.6	2.4	11.5	7.7	9.6	0.15	0.48	0.26
P3	0.21	5.1	3.1	2.0	14.6	9.7	12.1	0.06	0.25	0.12
P4	0.34	5.9	3.5	2.4	10.6	7.0	8.8	0.19	0.59	0.35

The dune shapes observed along each of the mid-channel profiles were regular and did not exhibit any systematic change in height and wavelength during the course of the ebb tide. The mean heights and wavelengths of the dunes (η_d, λ_d) averaged for each along-channel profile P1 to P4 were (0.47 m, 7.4 m), (0.32 m, 6.1 m), (0.21 m, 5.1 m) and (0.34 m, 5.9 m), respectively (see Table 3). However, a complete reorientation of the dune crest symmetry, from northeast facing to southwest facing, was measured over the course of the survey period. This was accompanied by the migration of the dune crests in the southwest direction by distances ranging from 0.4 m to 5.5 m. According to the broad regimes defined for tidal bedforms by Van Rijn (1993) (see Section 2) the present observations of (η_d, λ_d), with a representative sediment median grain size of 0.25 mm, would appear to be of 'mega-ripples'. However, Van Rijn's (2007) scheme used here predicts the bed roughness to be dominated by the dune contribution k_{sd}.

With the horizontal length of the dune lee slope taken as λ_1 and the dune height as η_d, values of the dune asymmetry ratio λ_1/η_d decreased from an overall mean value of 11.5 to 7.7 during the 5.5 hour survey period (see Table 3). The corresponding change in Van Rijn's form factor γ_d (see Section 2) was from an overall mean value of 0.17 to 0.51. At the onset of the ebb tide, the low value of γ_d resulted from the shallow lee slope left by the previous flood tide (cf. Rippeth et al. (2002)). As the dunes reoriented on the ebb tide, the lee slope steepened and γ_d increased to its final value of about 0.51. The

mean value of γ_d of 0.30 during this process was about one half of Van Rijn's (1993) expected value of 0.70 for dunes in field conditions. This provides a plausible explanation for the factor of 2 difference between the modelled k_s values which here are roughly equal to the observed dune heights and Van Rijn's expectation that k_{sd} should be 'roughly on the order of half the bedform height' (see Appendix A).
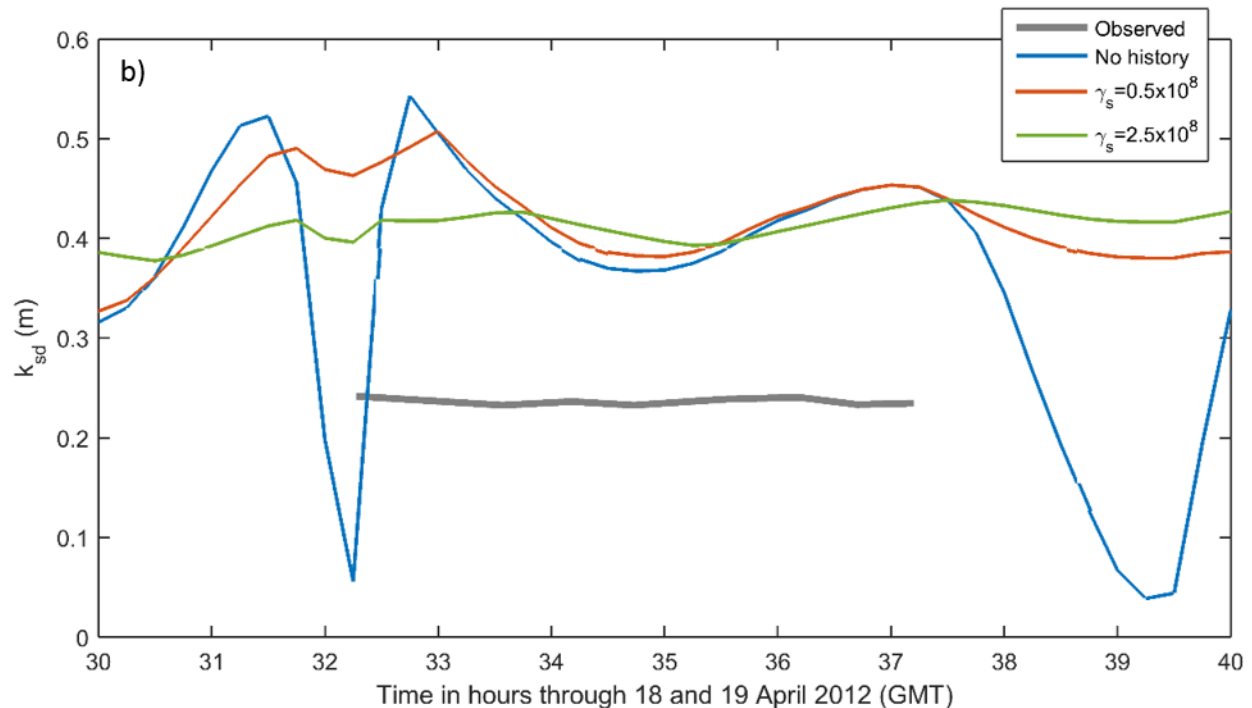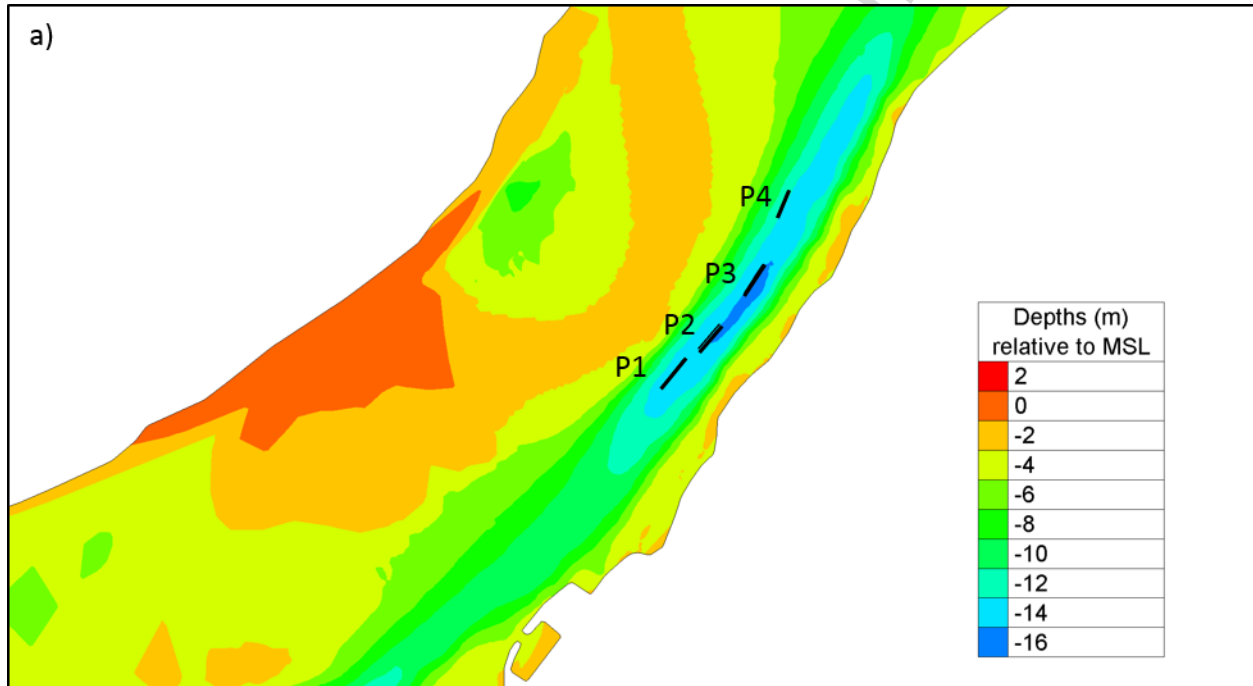

39

Figure 11. (a) Locations of the along-channel profiles P1 to P4 in the region of Traeth Gwyllt highlighted in Figure 1a. (b) Comparison between observed and predicted bed roughness for profile P1 over the survey period. The observed values show the dune roughness plotted in accordance with Van Rijn's assumption $k_{sd}=\eta_d/2$. The model outcomes are from a 2-day run covering 18th and 19th April 2012 during which dune observations were made between hours 32 and 38. The model results show the total k_s predicted without, and with, a 'history effect' applied.

The discrepancy arising from this assumption between the observations (plotted with $k_{sd}=0.5\eta_d$) and

model predictions of the dune roughness made with and without a 'history effect' applied are shown in

Fig. 11b for profile P1. Values of the development rate parameter γ_s were taken as 0.5×10^8 and 2.5×10^8.

Slack water at high and low tide occurred on site at hours 32.6 and 39.4, respectively. The model runs

were carried out with tidal inputs at either end of the Strait covering the survey period, with a run

duration of 2 days and a representative bed grain size of 0.25 mm. The use here of a mixture of grain

sizes (cf. Section 4.2), leading to some spatial variations in d_{50}, might have given rise to some minor

changes in the results in Fig. 11b. The predicted surface elevations were shown to match closely the

tidal curve measured on site. In the case of profile P1 for which the mean value of γ_d was 0.47, the

implied k_s value is about 0.57 times the modelled value averaged over the survey period. The

corresponding ratios for profiles P2, P3 and P4 were 0.41, 0.25 and 0.42, which can be seen in Table 3 to

be related to the respective values of λ_1/η_d. The model results in Fig. 11b show how the 'history effect'

suppresses the large temporal variations in k_s predicted at slack water both before and after the survey

period. As expected, the larger is the value of the maximum development rate parameter γ_s (Appendix

A) the more strongly damped is the temporal variation in k_s.

If it is accepted from the earlier water flux computations that Van Rijn's (2007) roughness predictor

gives a satisfactory representation of the bed friction, then it seems reasonable to suggest that in a

reversing tidal flow in which dunes attempt to form, but are not able to develop fully, Van Rijn's

predictor remains applicable but with the important caveat that k_{sd} is roughly on the order of the

bedform height, rather than half that height. This conclusion could possibly be refined through consideration of the role of the parameter λ_1/η_d. Values of λ_1/η_d in the approximate range 8 to 12 found in the present tidal setting are smaller than would be expected in a riverine setting (for which $\lambda_1/\eta_d \approx 6$ corresponds to Van Rijn's suggested value of $\gamma_d \approx 0.7$). This difference is associated with the more symmetrical bedforms that occur in reversing flow than in a comparable steady flow.

In summary, compared with dunes in river flow, the dunes observed by McAleese (2012) had (i) shorter wavelength (<h), (ii) more symmetrical profiles with less steep lee slopes and (iii) k_s on the order of the bedform height in most cases, rather than half the bedform height as suggested by Van Rijn (2007). However, the dunes being more numerous due to their smaller wavelength, they still exert significant frictional influence which seems to be well represented by Van Rijn's (2007) formulation subject to the caveat that in reversing tidal flow k_s/η_d is ≈ 1. The more symmetrical, more numerous, bedforms promote the turbulence intensity in the reversing flow and hence give rise to larger k_s values than would be expected in a river.

Finally, as noted in Section 4.2, the 'history effect' on the dune roughness k_{sd} inhibits intra-tidal changes in k_s, but still allows variations on a SN-timescale, though only limited observational evidence exists to support this latter supposition. Shaarani (2013) made further observations of dunes along the same survey profile lines P1 to P4 focussing on differences between spring and neap conditions. These observations suggested that dune lengths and heights were greater by 18% and 41%, respectively, on spring compared with neap tides. Such changes would appear to be consistent both with the observations reported by Rippeth et al. (2002) and also with the present prediction of k_s variations on this time scale, though more systematic observations are needed to tie down the value of development

rate parameter γ_s (see Appendix A). Further, the present 'history effect' takes no account of the variation of parameter λ_1/η_d on intra-tidal time scales, which could be incorporated in the formulation.

7. Conclusions

The use of a spatially and temporally variable, predicted, bed roughness k_s in coastal and estuarine morphodynamic modelling provides greater realism than the use of a constant, tuned value of k_s. This has been assessed by comparing Telemac modelling outcomes for a tidal channel (Menai Strait, N. Wales) obtained with variable k_s based on Van Rijn's (2007) prediction scheme, involving dunes, mega-ripples and small-scale ripples, with outcomes obtained for constant k_s values. Van Rijn's scheme has been accompanied by a new 'history effect' that prevents the dune roughness contribution from making unrealistically rapid, intra-tidal, changes.

The bed roughness scheme, available in the Telemac morphodynamic module Sisyphe, has been assessed by taking as a diagnostic the magnitude of the residual flow that occurs in the channel due to differences in tidal range and phase at its two open ends. Van Rijn's (2007) scheme predicts dune roughness in mid-channel tending to small-scale ripple roughness at the channel margins, as observed. The scheme also provides an accurate prediction of the residual flow that agrees with previous estimates and observations made in the Menai Strait. Compared with the use of a more traditional, constant k_s value to represent bottom friction throughout the model domain, variable k_s introduces subtle differences in the model outcomes, for example by slowing down the current speed in mid-channel while allowing greater speeds at the channel margins. Such differences, even if relatively small in magnitude, have the potential to alter long-term morphodynamic outcomes.

For a mean SN-cycle with variable k_s, the mean residual flow through the Menai Strait is predicted to be 525 m^3 s^{-1} towards the southwest, varying between 334 m^3 s^{-1} on neaps and 686 m^3 s^{-1} on springs, consistent with observations. With a constant k_s value imposed, this residual flow is recovered approximately using values of k_s in the range 0.2 m to 0.3 m. Such values are significantly smaller than the peak values of k_s predicted in the deeper water of the main channel, suggesting that the use of a mid-channel k_s value as an overall choice for the system may not be appropriate resulting, for this system at least, in an overstating of the residual flow. In fact, if the predicted spatially varying k_s is averaged throughout the Menai Strait this results in a value of about 0.15 m. So the effective roughness of the seabed ($k_s \approx$ 0.2-0.3 m) is less than half of the maximum local roughness due to the dunes predicted in mid-channel, but more than the spatially mean predicted k_s value in the Strait as a whole by about 50%.

The tidal simulations carried out for M_2-alone using variable k_s produced a somewhat smaller (by 7%) residual flow of 491 m^3 s^{-1} towards the southwest. The use of an 'equivalent M_2' tide of amplitude enhanced by 7.3% reconciled these estimates, suggesting that the residual flow magnitude is related approximately linearly to the M_2 tidal amplitude. Further, the unadjusted M_2-alone values can be recovered approximately by using constant k_s values in the range 0.1m to 0.3 m, an outcome similar to that found for the SN-cycle.

While Van Rijn's (2007) bed roughness scheme gives rise to the occurrence of dunes in the present tidal channel, the bedforms observed on site are smaller in height and length than predicted. This raises important questions about the applicability of roughness schemes developed for steady, riverine conditions in tidal conditions where repeated flow reversals prevent equilibrium dunes from forming. It may been concluded from the present study that, while Van Rijn's (2007) scheme provides a realistic

estimation of the roughness k_s, the relationship between k_s and the dunes on site differs from that occurring in a steady flow. In particular, k_{sd} appears to be roughly on the order of the bedform height in reversing flow, rather than half that height as expected in steady flow. This relationship arises from the dunes in the tidal setting being smaller in wavelength, but therefore more numerous, and at the same time more upright and symmetrical than dunes in a river. The dune behaviour in tidal flow seems also to involve significant intra-tidal changes in bedform profile asymmetry that alter the roughness and that could, potentially, be included to improve future models.

References

Allen, J.R.L., 1976. Computational models for dune time-lag: General ideas, difficulties, and early results. Sedimentary Geology 15, 1-53.

Atkins, R., Soulsby, R.L., Waters, C.B., Oliver, N., 1989. Field measurements of sediment suspension above bedforms in a sandy estuary. Hydraulics Research Wallingford Report SR 203, 21pp.

Bartholomä, A., Ernstsen, V.B., Flemming, B.W., Bartholdy, J., 2004. Bedform dynamics and net sediment transport paths over a flood-ebb tidal cycle in the Grådyb channel (Denmark), determined by high-resolution multibeam echosounding. Danish Journal of Geography 104 (1), 45-55.

Best, J., 2005. The fluid dynamics of river dunes: A review and some future research directions. Journal of Geophysical Research 110, F04S02, doi:10.1029/2004JF000218.

Bijker, E.W., 1992. Mechanics of sediment transport by the combination of waves and current. Proceedings of the 23rd International Conference on Coastal Engineering, American Society of Civil Engineers, Venice, Italy, 147-173.

Bowers, D.G., Macdonald, R.G., McKee, D., Nimmo-Smith, W.A.M., Graham, G.W., 2013. On the formation of tide-produced seiches and double high waters in coastal seas. Estuarine, Coastal and Shelf Science 134, 108-116.

Campbell, A.R., Simpson, J.H., Allen, G.L., 1998. The dynamical balance of flow in the Menai Strait. Estuarine, Coastal and Shelf Science 46, 449-455.

Canadian Hydraulics Centre, 2011. Blue Kenue^{TM} : Software tool for hydraulic modellers. National Research Council of Canada.

http://www.nrc-cnrc.gc.ca/eng/solutions/advisory/blue_kenue_index.html

Coleman, S.E., Zhang, M.H., Clunie, T.M., 2005. Sediment-wave development in subcritical water flow. Journal of Hydraulic Engineering 131 (2), 106-111.

Dalrymple, R.W., Mackay, D.A., Ichaso, A.A., Choi, K.S., 2012. Process, morphodynamics, and facies of tide-dominated estuaries. In: Davis, R.A., Dalrymple, R.W. (Eds.), Principles of tidal sedimentology, Springer Science+Business Media B.V., pp. 79-107. doi:10.1007/978-94-007-0123-6_5.

Davies, A.G., Thorne, P.D., 2008. Advances in the Study of Moving Sediments and Evolving Seabeds. Surveys in Geophysics 29, 1-36. doi:10.1007/s10712-008-9039-x.

Available at: http://dx.doi.org/10.1007/s10712-008-9039-x

Davies, A.G., Villaret, C., 2002. Prediction of sand transport rates by waves and currents in the coastal zone. Continental Shelf Research 22 (18-19), 2725-2737.

Doré, A., Bonneton, P., Marieu, V., Garlan, T., 2016. Numerical modeling of subaqueous sand dune morphodynamics. Journal of Geophysical Research Earth Surface 121, 565-587. doi:10.1002/2015JF003689.

Engelund, F., 1978. Hydraulic resistance for flow over dunes. I.S.V.A., Technical University of Denmark, Progress Report No. 44.

Fredsøe, J., 1979. Unsteady flow in straight alluvial streams: modification of individual dunes. Journal of Fluid Mechanics 91 (3), 497-512.

Fredsøe, J., 1982. Shape and dimensions of stationary dunes in rivers. Journal of the Hydraulics Division, Proceedings of the Society of Civil Engineers, A.S.C.E., HY8, 932-947.

Fredsøe, J., Deigaard, R., 1992. Mechanics of coastal sediment transport. Advanced Series on Ocean Engineering 3. World Scientific, Singapore, 369pp.

George, K., 2006. Tide-watching, cubature and friction in the Menai Strait. The Hydrographic Journal 118, 10-16.

George, K., 2007. A depth-averaged tidal numerical model using non-orthogonal curvilinear co-ordinates. Ocean Dynamics 57, 363-374.

Harvey, J.G., 1968. The flow of water through the Menai Straits. Geophysical Journal of the Royal Astronomical Society 15, 517-528.

Hervouet, J.-M., 2007. Hydrodynamics of free surface flows, Modelling with the finite-element method. John Wiley and Sons Ltd., West Sussex, England. 340pp.

Johns, B., Soulsby, R.L., Xing, J., 1993. A comparison of numerical model experiments of free surface flow over topography with flume and field observations. Journal of Hydraulic Research 31 (2), 215-228.

Julien, P.Y., Klaassen, G.J., Ten Brinke, W.B.M., Wilbers, A.W E., 2002. Case study: Bed resistance of Rhine River during 1998 flood. Journal of Hydraulic Engineering 128 (12), 1042-1050.

Kostaschuk, R., Best, J., 2005. Response of sand dunes to variations in tidal flow: Fraser Estuary, Canada. Journal of Geophysical Research 110, F04S04, doi:10.1029/2004JF000176.

Kwoll, E., Venditti, J.G., Bradley, R.W., Winter, C., 2016. Flow structure and resistance over subaquaeous high- and low-angle dunes. Journal of Geophysical Research Earth Surface 121, 545-564. doi:10.1002/2015JF003637.

Latteux, B., 1995. Techniques for long-term morphological simulation under tidal action. Marine Geology, 126 (1-4), 129-141.

Lefebvre, A., Ernstsen, V.B., Winter, C., 2011. Influence of compound bedforms on hydraulic roughness in a tidal environment. Ocean Dynamics 61, 2201-2210. doi:10.1007/s10236-011-0476-6.

Lefebvre, A., Ernstsen, V.B., Winter, C., 2013. Estimation of roughness lengths and flow separation over compound bedforms in a natural tidal inlet. Continental Shelf Research 61-62, 98-111.

Lefebvre, A., Paarlberg, A.J., Ernstsen, V.B., Winter, C., 2014. Flow separation and roughness lengths over large bedforms in a tidal environment: A numerical investigation. Continental Shelf Research 91, 57-69.

Lefebvre, A., Paarlberg, A.J., Winter, C., 2016. Characterising natural bedform morphology and its influence on flow. Geo-Marine Letters 36, 379-393. doi:10.1007/s00367-016-0455-5.

Lefebvre, A., Winter, C., 2016. Predicting bed form roughness: the influence of lee side angle. Geo-Marine Letters 36, 121-133. doi:10.1007/s00367-016-0436-8.

Lewis, M.J., Neill, S.P., Robins, P.E., Hashemi, R.M., 2015. Resource assessment for future generations of tidal-stream energy arrays. Energy 83, 403-415.

Li, M., Pan, S., O'Connor, B.A., 2006. Modelling coastal boundary layer flows over typical bed-forms. Proceedings of the Institution of Civil Engineers, Maritime Engineering 159 (MA1), 9-24.

McAleese, G., 2012. Monitoring subaqueous sand dune evolution in response to tidal motions. MSc thesis, Bangor University, 120pp.

McCann, D.L., Davies, A.G., Bennell, J.D., 2011. Bed roughness feedback in TELEMAC-2D and SISYPHE. Proceedings of XVIIIth Telemac & Mascaret User Club, 19-21 October 2011, Chatou, France, 99-104.

Mendoza, A., Abad, J.D., Langendoen, E.J., Wang, D., Tassi, P., Abderrezzak, K.E.K., 2017. Effect of sediment transport boundary conditions on the numerical modeling of bed morphodynamics. Journal of Hydraulic Engineering 143 (4). doi:10.1061/(ASCE)HY.1943-7900.0001208.

Niemann, S. L., Fredsøe, J., Jacobsen, N.G., 2011. Sand dunes in steady flow at low Froude numbers: dune height evolution and flow resistance." Journal of Hydraulic Engineering 137 (1), 5-14.

Paarlberg, A.J., Dohmen-Janssen, C.M., Hulscher, S.J.M.H., Berg, J. van den, Termes, A.P.P., 2006. *Modelling morphodynamic evolution of river dunes.* In: Rui M.L. Ferreira (Ed.), River flow 2006 : proceedings of the International Conference on Fluvial Hydraulics, Lisbon, Portugal, 6-8 September 2006. Taylor & Francis, London. ISBN 9780415408158

47

Paarlberg, A.J., Dohmen-Janssen, C.M., Hulscher, S.J.M.H., Termes, A.P.P., 2009. Modeling river dune evolution using a parameterization of flow separation. Journal of Geophysical Research 114, F01014, doi:10.1029/2007/JF000910

Paarlberg, A.J., Dohmen-Janssen, C.M., Hulscher, S.J.M.H., Termes, A.P.P., Schielen, R., 2010. Modelling the effect of time-dependent river dune evolution on bed roughness and stage. Earth Surface Processes and Landforms 35, 1854-1866.

Parsons, D. R., Best, J.L., Orfeo, O., Hardy, R.J., Kostaschuk, R., Lane, S.N., 2005. Morphology and flow fields of three-dimensional dunes, Rio Paraná, Argentina: Results from simultaneous multibeam echo sounding and acoustic Doppler current profiling. Journal of Geophysical Research 110, F04S03. doi:10.1029/2004JF000231

Rippeth, T.P., Williams, E., Simpson, J.H., 2002. Reynolds stress and turbulent energy production in a tidal channel. Journal of Physical Oceanography 32, 1242-1251.

Roberts, M.J., Scourse, J.D., Bennell, J.D., Huws, D.G., Jago, C.F., Long, B.T., 2011. Journal of Quaternary Science 26 (2), 141-155.

Shaarani, N.A., 2013. Monitoring subaqueous sand dune evolution in response to tidal motions, Traeth Gwyllt, Menai Strait. MSc thesis, Bangor University, 135pp.

Simpson, J.H., Forbes, A.M.G., Gould, W.J., 1971. Electromagnetic observations of water flow in the Menai Straits. Geophysical Journal of the Royal Astronomical Society 24, 245-253.

Soulsby, R.L., 1990. Tidal-Current Boundary Layers. In The Sea, Volume 9, Part A, Ed. B. Le Méhauté and D.M. Hanes, Wiley Interscience, New York, pp. 523-566.

Van Duin, O. J. M., Hulscher, S.J.M.H., Ribberink, J.S., Dohmen-Janssen, C.M., 2017. Modeling of spatial lag in bed-load transport processes and its effect on dune morphology. Journal of Hydraulic Engineering 143 (2). doi:10.1061/(ASCE)HY.1943-7900.0001254.

Van Rijn, L.C., 1993. Principles of sediment transport in rivers, estuaries and coastal seas. Aqua Publications, Amsterdam, The Netherlands, ISBN 90-800356-2-9.

Van Rijn, L.C., 2007. Unified view of sediment transport by currents and waves. 1 Initiation of motion, bed roughness and bed-load transport. Journal of Hydraulic Engineering 133 (6), 649-667.

Venditti, J. G., Lin, C.-Y.M., Kazemi, M., 2016. Variability in bedform morphology and kinematics with transport stage. Sedimentology 63, 1017-1039.

Villaret, C., Huybrechts, N., Davies, A.G., Way, O., 2011. Effect of bed roughness prediction on morphodynamic modelling: Application to the Dee estuary (UK) and to the Gironde estuary (France). Proceedings of the 34th World Congress of the International Association for Hydro-

Environment Research and Engineering: 33rd Hydrology and Water Resources Symposium and 10th Conference on Hydraulics in Water Engineering, 2011, p.1149-1156 (ISBN: 9780858258686)

Villaret, C., Huybrechts, N., Davies, A.G., 2012. A large scale morphodynamic process-based model of the Gironde estuary. In: *NCK-days 2012 : Crossing borders in coastal research*, 13 March 2012 - 16 March 2012, Enschede, the Netherlands, 8pp. ISBN 9789036533423

Villaret, C., Hervouet, J-M., Kopmann, R., Merkel, U., Davies, A.G., 2013. Morphodynamic modelling using the Telemac finite element system. Computers & Geosciences 53, 105-113.

Wilbers, A.W.E., Ten Brinke, W.B.M., 2003. The response of subaqueous dunes to floods in sand and gravel bed reaches of the Dutch Rhine. Sedimentology 50, 1013-1034.

Zorndt, A.C., Wurpts, A., Schlurmann, T., 2011. The influence of hydrodynamic boundary conditions on characteristics, migration, and associated sand transport of sand dunes in a tidal environment. Ocean Dynamics 61, 1629-1644.

Appendix A

Bed roughness prediction, 'history effect' and modelling methodology

The formulation of Van Rijn (2007) was used to determine the roughness of sub-grid-scale bed features. The roughness concept may be traced back to the equivalent sand roughness height (k_s) of Nikuradse which, in the case of a movable bed of sediment, is subdivided into the grain roughness ($k_s' = k_{s,grain}$) arising from skin friction forces and form roughness (k_s'') generated by pressure forces acting on the bedforms.

A.1 Quasi-steady bed roughness prediction

Van Rijn's (2007) formulation for the bed roughness contributions arising from small-scale ripples k_{sr}, mega-ripples k_{smr} and dunes k_{sd} depends upon a single parameter, namely the mobility number, defined in the absence of waves as:

$$\psi = U_c^2 / \{(s-1)gd\} \qquad (A.1)$$

where U_c is the depth-mean current speed; $s = \rho_s / \rho$ is the relative sediment density (ρ_s and ρ are the densities of sediment and water respectively); g is the acceleration due to gravity; and $d = d_{50}$ is the median grain diameter. An example of results from the predictor is given in Fig. A1. [If waves are present U_c^2

is replaced by $(U_c^2 + U_w^2)$ where U_w is the near-bed wave velocity amplitude.]

The local instantaneous roughness contributions were computed in Sisyphe, as follows:

i)   the roughness of movable small-scale ripples (k_{sr}) is assumed to be equal approximately to the ripple height. The ripples are assumed to be 'fully developed' and so growth and history effects are not

50

included. The 'smooth' formula proposed by Van Rijn (2007) to represent k_{sr} over the full ψ-range is as follows:

$$k_{sr} = f_{cs}d_{50}\{85 - 65tanh[0.015(\psi - 150)]\} \qquad (A.2)$$

where either the coefficient $f_{cs} = \left(0.25\,d_{gravel}/d_{50}\right)^{1.5}$ with $d_{gravel} = 0.002$ m, or $f_{cs} = 1$ for $d_{50} \leq 0.25d_{gravel}$. For fine sediment of silt size a separate expression is used:

$$k_{sr} = 20d_{silt} \text{ for } d_{50} < d_{silt} \text{ where } d_{silt} = 0.000032\,m \qquad (A.3)$$

The predicted ripple roughness is maximum in the lower current regime, while the ripples are suppressed at high flow stages, ultimately disappearing in the upper current regime ($\psi \geq 250$).

ii)   mega-ripples (k_{smr}) have a different behavior in that they tend first to increase in height, and then decrease, for increasing ψ. The wavelengths of mega-ripples are of the order of, but no greater than, the mean water depth (h). Van Rijn (2007) indicates that the roughness (k_{smr}) is 'roughly on the order of half the bedform height'. Thus the dominance of small-scale ripples at low wave-current mobility is replaced, in part, by the presence of mega-ripples at higher mobility. Van Rijn's (2007) direct parameterisation of k_{smr} over the full ψ-range is as follows:

$$k_{smr} = 0.00002f_{fs}h[1 - exp(-0.05\,\psi)](500 - \psi) \qquad (A.4)$$

where the factor $f_{fs} = d_{50}/1.5d_{sand}$ where $d_{sand} = 0.000062\,m$, or $f_{fs} = 1$ for $d_{50} \geq 1.5d_{sand}$. At high flow stages the following expressions are used:

$$k_{smr} = 0.02 \text{ m for } \psi > 550 \text{ and } d_{50} \geq 1.5d_{sand}$$

$$(A.5)$$

$$k_{smr} = 200d_{50} \text{ for } \psi > 550 \text{ and } d_{50} < 1.5d_{sand}$$

For fine sediment of silt size the mega-ripples are inhibited:

$$k_{smr} = 0 \text{ for } d_{50} < d_{silt} \qquad (A.6)$$

51

iii)   dunes (k_{sd}) have different characteristics compared with mega-ripples, mainly by being strongly dependent upon the water depth (h) and having wavelengths larger than the depth (in the range 3h to 15h).   The dunes achieve significant heights and, like mega-ripples, induce form roughness.   Also like mega-ripples they first increase, and then decrease, in height for increasing mobility. As for mega-ripples, Van Rijn (2007) indicates that the physical bedform roughness (k_{sd}) of dunes is 'roughly on the order of half the bedform height'.   The formula proposed by Van Rijn (2007) for the full ψ-range is:

$$k_{sd} = 0.00008 f_{fs} h[1 - exp(-0.02\psi)](600 - \psi) \qquad (A.7)$$

where the factor f_{fs} is as defined earlier.   For high mobility and for fine-grained sediment, the dunes are inhibited:

$$k_{sd} = 0 \quad \text{for} \quad \psi > 600 \quad \text{and for} \quad d_{50} < d_{silt} \qquad (A.8)$$

The above formulation allows maximum k_{sd} values to increase as h increases up to a maximum allowed value of $k_{sd} = 1\,m$.   The dune roughness typically far exceeds the contributions made to the total roughness by mega-ripples and small-scale ripples.

iv)   The overall roughness due to the respective sub-grid-scale features, which may be superimposed upon one another in the coastal domain, is obtained by quadratic summation:

$$k_{s,TOT} = \left[k_{sr}^2 + k_{smr}^2 + k_{sd}^2\right]^{\frac{1}{2}} \qquad (A.9)$$

This quadratic expression, rather than a simple summation, is acknowledged by Van Rijn (2007) to be an intuitive, engineering approach.   It is possibly justified for situations where the bedform crest lines are not aligned, such that flows directed, locally and instantaneously, along crests (and troughs) of one or other of the bedform components will not encounter the full roughness of that component but, instead, a sharply reduced value (cf. Soulsby, 1990).   Thus a simple addition of the three roughness components to determine $k_{s,TOT}$ might lead to an overestimate.

The total roughness is calculated in Sisyphe at each point of the computational domain, using equations (A.1) – (A.9); to the quadratic summation in equation (A.9) is added a granular, skin friction, component k'_s . The total roughness is passed back from Sisyphe to Telemac2D. The flow calculated in Telemac2D adjusts to the evolving roughness and the velocity field is passed back in turn to Sisyphe.   This interaction between the modules has been robust and stable in all simulations carried out to date. The sediment transport calculations in Sisyphe use only the small-scale ripple roughness k_{sr} (Equations (A.2) –(A.3)) together with skin friction effects (k'_s) that are worked out here according to Bijker's (1992) transport formulation (see Davies and Villaret, 2002).

A.2 History effect for dune roughness

The quasi-steady application of the earlier formulae through a tidal cycle implies an equilibrium response of the bed roughness to changes in the flow conditions. In practice, such a rapid response may be unrealistic due to the time required for bedforms to grow or to be destroyed. In other words, there is a 'history effect' in the bedform response. Here only the dune roughness component is considered, though the same principle and methodology may be applicable also to mega-ripples. The aim of the new 'history effect' is to inhibit the rate of bedform growth/destruction in a realistic manner.

The time scale of dune evolution will depend upon the strength of the flow U, the sediment grain size d (= d_{50}), the mean water depth h, and possibly also the acceleration due to gravity g, allowing a Froude number dependence. So, for example, the time scale T_d for the growth of a dune might be governed by $T_d \sim {d}/{U}$ such that the larger the grains the longer the time scale, and the larger the velocity the shorter the time scale. Suppose that it takes, for example, about 6 hours $\cong 2 \times 10^4$ s for 'equilibrium', i.e. fully developed, dunes to form in a current of strength 1 m/s for a grain diameter of d = 0.2 mm = 2×10^{-4} m, then ${d}/{U} = 2 \times 10^{-4}\, s$ and $T_d = {d}/{U} \times \gamma_s$ s   with constant $\gamma_s \sim O(10^8)$. Such a time scale

53

provides the simplest possible basis upon which to define a lag effect, or 'history effect', for dune growth or erosion. If the quasi-steady approach to the calculation of k_s implies a dune growth/destruction rate that is faster than that which can possibly be attained according to the time scale T_d, then the growth/destruction rate of the dunes should be inhibited. It is assumed in the algorithm applied here that there is no distinction between inhibition on growth and that on destruction.

New procedures have been introduced into Sisyphe to implement the dune 'history effect'. Suppose that the existing bed roughness at a typical grid node within the domain is denoted by $k_{s,now}$. At the next iteration (after interval Δt) the model computes a new, quasi-steady, set of equilibrium values of the bed roughness $k_{s,eq}$, say, based on the mobility number ψ at each grid node. For the bedforms to develop at the rate implied by this equilibrium value, the bed roughness k_s needs to change at the 'target' rate:

$\frac{\Delta k_s}{\Delta t} = \frac{k_{s,eq} - k_{s,now}}{\Delta t}$ which, according to Van Rijn's (2007) rule (Section 6), implies a 'target' rate of change

of dune height η_d of $2 \times \frac{\Delta k_s}{\Delta t}$. The question that arises is whether this target rate is greater than the maximum allowable growth rate for the existing flow state (i.e. stage of the tide), namely:

$$\frac{\eta_{d,eq}}{T_d} = \frac{2k_{s,eq}}{T_d} = \frac{2k_{s,eq}}{\left(\gamma_s d / U \right)} \qquad (A.10)$$

The new algorithm limits the dune growth or destruction rate to be no greater than the maximum allowable rate, at that that location, and at that time.

A.3 Implementation of the 'history effect' in Sisyphe

Consider the case of a growing dune. If it takes time T_d for a dune of wavelength λ_d to grow to equilibrium (height $\eta_{d,eq}$) then the assumed maximum growth rate for dune height is $\frac{\eta_{d,eq}}{T_d}$. If the target

54

growth rate $\frac{\Delta k_s}{\Delta t}$ is compared with $\frac{\frac{1}{2}\eta_{d,eq}}{T_d}$ then the following 'history effect' is imposed at that location in the domain:

$$k_s|_{t+1} = k_{s,eq} \quad \text{if} \quad \left|\frac{\Delta k_s}{\Delta t}\right| \leq \frac{k_{s,eq}}{T_d} = \frac{\frac{1}{2}\eta_{d,eq}}{T_d} \tag{A.11a}$$

or

$$k_s|_{t+1} = k_s|_t + (k_{s,eq} - k_s|_t) \times \left\{ \frac{\frac{\eta_{d,eq}}{2T_d}}{\frac{\Delta k_s}{\Delta t}} \right\}^R \quad \text{if} \quad \left|\frac{\Delta k_s}{\Delta t}\right| > \frac{\frac{1}{2}\eta_{d,eq}}{T_d} \tag{A.11b}$$

with the rate given by power R set to 1 as a first guess, which seems applicable if $\frac{\frac{1}{2}\eta_{d,eq}}{T_d}$ is specified as a function of the flow speed. A schematic of inhibited roughness growth is depicted in Fig. A2. An equivalent procedure has been programmed for decaying dunes.

The implementation requires knowledge of the roughness values $k_s|_t$ at the old time step. At each iteration of Sisyphe the newly calculated roughness values have been retained for further use. At the next iteration of Sisyphe, these values $k_{s,now}$ are used to determine the target dune growth rate $\frac{\Delta k_s}{\Delta t} = \frac{k_{s,eq} - k_{s,now}}{\Delta t}$ and, hence, the history effect in the roughness (via Equation (A.11)). The procedure appears to be numerically robust and stable, and it is also physically meaningful. What is still needed is additional site information with which to tune the calibration constant γ_s (and also, subsequently, R), and to determine whether growth and decay can really be characterized by the same time scale T_d or whether two different time scales are needed.
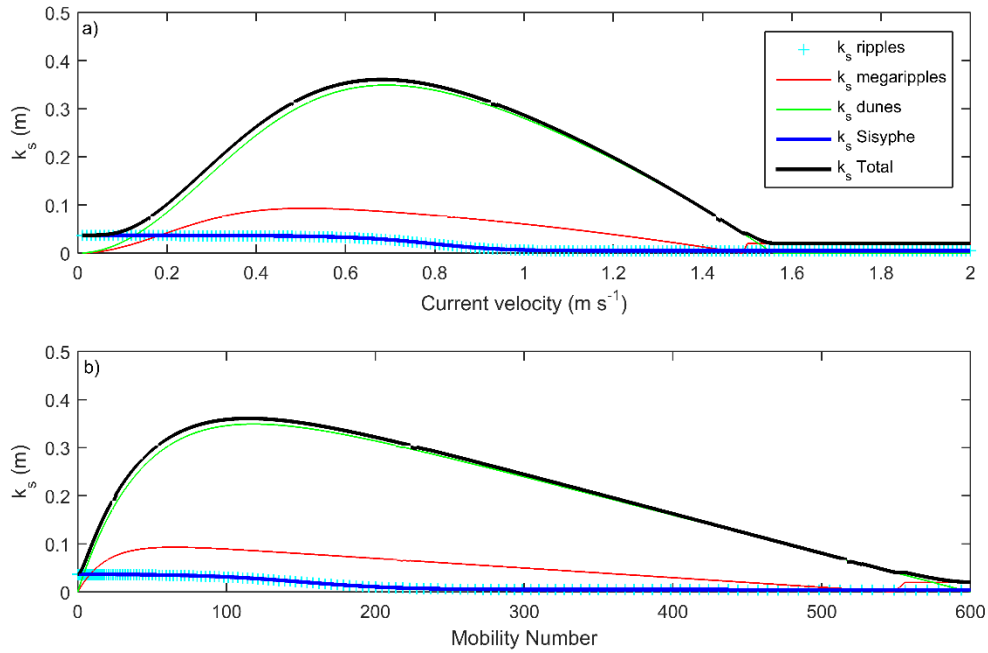
Figure A1. Roughness contributions for water depth 10 m, median grain diameter 0.00025 m and current speeds in the range 0 to 2 m s^{-1}. The dominance of dune roughness is apparent, as is the relative importance of small-scale ripple roughness for low values of mobility number ψ.
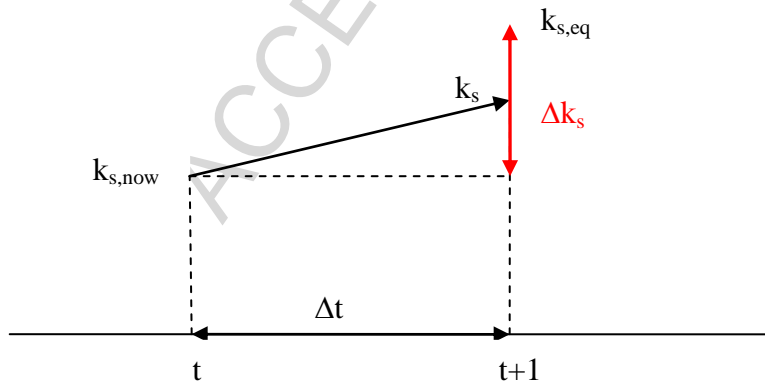

Figure A2. Scheme for 'history effect' in the case of a growing dune showing the instantaneous target $k_{s,eq}$ at the next time step, together with the imposed value k_s implying an inhibition in the rate of change of the roughness.

Highlights:

• Flow in tidal channel modelled with temporally/spatially varying bed roughness.

• Comparisons made between Telemac simulations using variable and fixed bed roughness.

• Residual flow in channel used as diagnostic to assess different roughness formulations.

• New 'history effect' applied in prediction of dune roughness in reversing tidal flow.

• Predicted bed roughness found to equal approximately dune height on site.